

# UC Davis

## UC Davis Previously Published Works

### Title

Single Nucleotide Polymorphism rs9277336 Controls the Nuclear Alpha Actinin 4-Human Leukocyte Antigen-DPA1 Axis and Pulmonary Endothelial Pathophenotypes in Pulmonary Arterial Hypertension

### Permalink

<https://escholarship.org/uc/item/1dq366dn>

### Journal

Journal of the American Heart Association, 12(7)

### ISSN

2047-9980

### Authors

Hafeez, Neha  
Kirillova, Anna  
Yue, Yunshan  
[et al.](#)

### Publication Date

2023-04-04













### DOI

10.1161/jaha.122.027894

Peer reviewed

## ORIGINAL RESEARCH

# Single Nucleotide Polymorphism rs9277336 Controls the Nuclear Alpha Actinin 4-Human Leukocyte Antigen-DPA1 Axis and Pulmonary Endothelial Pathophenotypes in Pulmonary Arterial Hypertension

Neha Hafeez , BS; Anna Kirillova , BS; Yunshan Yue; Rashmi J. Rao, BA; Neil J. Kelly , MD, PhD; Wadih El Khoury , MD; Yassmin Al Aaraj, MD; Yi-Yin Tai, MS; Adam Handen, MS; Ying Tang, MS; Danli Jiang, PhD; Ting Wu, PhD; Yingze Zhang , PhD; Dennis McNamara, MD; Tatiana V. Kudryashova , PhD; Elena A. Goncharova , PhD; Dmitry Goncharov, MS; Thomas Bertero , PhD; Mehdi Nouraie , MD, PhD; Gang Li , PhD; Wei Sun , MD,\*; Stephen Y. Chan , MD, PhD\*

**BACKGROUND:** Pulmonary arterial hypertension (PAH) is a complex, fatal disease where disease severity has been associated with the single nucleotide polymorphism (SNP) rs2856830, located near the human leukocyte antigen DPA1 (HLA-DPA1) gene. We aimed to define the genetic architecture of functional variants associated with PAH disease severity by identifying allele-specific binding transcription factors and downstream targets that control endothelial pathophenotypes and PAH.

**METHODS AND RESULTS:** Electrophoretic mobility shift assays of oligonucleotides containing SNP rs2856830 and 8 SNPs in linkage disequilibrium revealed functional SNPs via allele-imbalanced binding to human pulmonary arterial endothelial cell nuclear proteins. DNA pulldown proteomics identified SNP-binding proteins. SNP genotyping and clinical correlation analysis were performed in 84 patients with PAH at University of Pittsburgh Medical Center and in 679 patients with PAH in the *All of Us* database. SNP rs9277336 was identified as a functional SNP in linkage disequilibrium ( $r^2 > 0.8$ ) defined by rs2856830, and the minor allele was associated with decreased hospitalizations and improved cardiac output in patients with PAH, an index of disease severity. SNP pulldown proteomics showed allele-specific binding of nuclear ACTN4 (alpha actinin 4) protein to rs9277336 minor allele. Both ACTN4 and HLA-DPA1 were downregulated in pulmonary endothelium in human patients and rodent models of PAH. Via transcriptomic and phenotypic analyses, knockdown of HLA-DPA1 phenocopied knockdown of ACTN4, both similarly controlling cell structure pathways, immune pathways, and endothelial dysfunction.

**CONCLUSIONS:** We defined the pathogenic activity of functional SNP rs9277336, entailing the allele-specific binding of ACTN4 and controlling expression of the neighboring HLA-DPA1 gene. Through inflammatory or genetic means, downregulation of this ACTN4-HLA-DPA1 regulatory axis promotes endothelial pathophenotypes, providing a mechanistic explanation for the association between this SNP and PAH outcomes.

**Key Words:** endothelial dysfunction ■ genome-wide association study ■ linkage disequilibrium ■ pulmonary arterial hypertension ■ single nucleotide polymorphism

Correspondence to: Stephen Y. Chan, MD, PhD and Wei Sun, MD, Center for Pulmonary Vascular Biology and Medicine, Pittsburgh Heart, Lung, and Blood Vascular Medicine Institute, Division of Cardiology, University of Pittsburgh Medical Center, 200 Lothrop Street BST E1240, Pittsburgh, PA.

Email: [chansy@pitt.edu](mailto:chansy@pitt.edu); [sunw2@upmc.edu](mailto:sunw2@upmc.edu)

\*W. Sun and S. Y. Chan contributed equally.

Supplemental Material is available at <https://www.ahajournals.org/doi/suppl/10.1161/JAHA.122.027894>

For Sources of Funding and Disclosures, see page 16.

© 2023 The Authors. Published on behalf of the American Heart Association, Inc., by Wiley. This is an open access article under the terms of the [Creative Commons Attribution-NonCommercial](#) License, which permits use, distribution and reproduction in any medium, provided the original work is properly cited and is not used for commercial purposes.

JAHA is available at: [www.ahajournals.org/journal/jaha](http://www.ahajournals.org/journal/jaha)

## CLINICAL PERSPECTIVE

### What Is New?

- Guided by prior genome-wide association study data coupled with proteomic analysis, single nucleotide polymorphism rs9277336, located near human leukocyte antigen DPA1, is associated with improved clinical prognostic markers of pulmonary arterial hypertension and binds in an allele-specific manner to ACTN4 (alpha actinin 4).
- This study provides a streamlined approach by which to identify functional single nucleotide polymorphisms and binding partners that drive downstream changes that explain results from genome-wide association studies.
- This study leverages large patient databases to determine associations of functional single nucleotide polymorphisms with clinical outcomes, including hospitalization.

### What Are the Clinical Implications?

- Human leukocyte antigen-DPA1 and ACTN4 are newly identified pathogenic regulators in pulmonary arterial hypertension that can inform potential diagnostics and therapeutics in pulmonary arterial hypertension in the future.
- This approach can be broadly applied to other variants in pulmonary arterial hypertension as well as a multitude of other diseases, allowing for significant advancement in our understanding and application of genome-wide association studies in clinical practice.
- This study provides a basis for a future personalized medicine approach using patient genomic sequencing to drive targeted management.

## Nonstandard Abbreviations and Acronyms

<b>ACTN4</b>	alpha actinin 4
<b>CLDN1</b>	claudin 1
<b>LD</b>	linkage disequilibrium
<b>PAEC</b>	pulmonary arterial endothelial cell
<b>PAH</b>	pulmonary arterial hypertension
<b>UPMC</b>	University of Pittsburgh Medical Center

**P**ulmonary arterial hypertension (PAH) is a complex, progressive disease characterized by pulmonary arterial dysfunction and pulmonary vascular stiffening.<sup>1</sup> PAH cases are driven by a combination of altered genetic susceptibility and environmental pathogenic triggers, such as hypoxia or inflammatory factors. Increasing evidence supports a primary and causative inflammatory component in PAH, marked by increased cytokines and

autoantibodies as well as association with inflammatory conditions such as scleroderma and HIV.<sup>2,3</sup> In the past 2 decades, substantial advances have been made in our understanding of the genetic predisposition to PAH pathogenesis.<sup>4</sup> Pathogenic mutations in specific genes, such as *BMPR2* (bone morphogenetic protein receptor 2), predispose individuals to PAH, particularly in heritable or familial PAH. These coding gene mutations, however, are considered as rare variants and found in only a small portion (<5%) of patients with PAH.<sup>5</sup> Although multiple efforts have been applied to investigate the roles of acquired PAH factors, it remains challenging to elucidate the mechanisms underlying the genetic susceptibility of PAH and how altered genetic susceptibility interacts with acquired environmental factors to trigger the pathogenesis of PAH.

In complex diseases such as PAH, disease trait-associated single nucleotide polymorphisms (SNPs) are increasingly viewed as determinants that control genetic disease susceptibility.<sup>6,7</sup> Genome-wide association studies (GWAS) have been instrumental in defining associations between such SNPs and disease occurrence or severity in large patient and control cohorts.<sup>8,9</sup> Since 2013, several PAH GWAS have been conducted and have identified 9 PAH-associated loci.<sup>10–15</sup> Most of these PAH GWAS, however, included only small cohorts and geographically localized population, mainly because of the rarity of the disease. In 2019, the largest global meta-analysis of PAH GWAS was published, which encompassed 2085 patients with PAH and 9659 controls across Europe and North America. In this GWAS, a group of noncoding genetic variants led by tag SNP rs2856830 near the human leukocyte antigen DPA1 (*HLA-DPA1*) gene was found to be associated with improved survival among patients with PAH, based on years of survival from diagnosis (median survival 13.50 years [95% CI, 12.07 to >13.50] compared with 6.97 years [95% CI, 6.02–8.05], odds ratio=1.56,  $P=7.65 \times 10^{20}$ ), despite similar baseline disease severity.<sup>15</sup>

*HLA-DPA1* is part of the HLA family of genes, which encode for major histocompatibility complexes Class I and Class II and are involved in antigen presentation to immune cells. Variants of genome-wide significance in *HLA-DPA1* have been associated with autoimmune diseases such as ankylosing spondylitis and inflammatory bowel disease,<sup>16–18</sup> which are diseases with known links to PAH.<sup>19–21</sup> Similarly, reduced expression of *HLA-DP* genes has been implicated in inflammatory conditions like multiple myeloma,<sup>22</sup> as well as other vascular diseases such as preeclampsia.<sup>23,24</sup> However, to our best knowledge, *HLA-DPA1* has not been previously mechanistically linked with pulmonary hypertension. Given its clinical relevance from the GWAS study, *HLA-DPA1* is a unique target that could provide more insights into the genomics underlying PAH pathogenesis.

Little is known at the molecular or mechanistic level regarding if or how the tag SNP rs2856830, a non-coding intronic genetic variant, may be causatively linked to PAH. This is because GWAS only reveal statistical associations without elucidating the biological mechanisms. Furthermore, to date, no causative pathobiology in PAH has been ascribed to tag SNP rs2856830. Notably, because certain SNPs are in high linkage disequilibrium (LD) with one another, the tag SNP rs2856830 originally reported by GWAS may not actually be functional or drive the observed association. Rather, this tag SNP may simply be linked to a true disease-causing, functional SNP (fSNP). These barriers have stalled the development of post-GWAS strategies to define the biological mechanisms underlying the statistical associations between these genetic variants and PAH pathogenesis and identify relevant molecular targets for PAH diagnostics and intervention.

To overcome these obstacles, we leveraged a recently developed post-GWAS functional genomics approach to identify and characterize disease-associated fSNPs.<sup>25–27</sup> This strategy is predicated on the fact that most of the disease-associated fSNPs in the noncoding region exert their functions by binding to regulatory proteins modulating risk gene expression. This approach includes screening of candidate fSNPs from a library of haplotype SNPs via electrophoretic mobility shift assay coupled with SNP-specific DNA competition pulldown-mass spectrometry and allele-imbalanced DNA pull-down Western blot for identification of the regulatory nuclear proteins that are associated with fSNPs. Using this approach, we screened the GWAS-reported PAH-associated SNP rs2856830 with its linked SNP haplotypes to identify an fSNP and its associated regulatory factors. Such PAH pathogenic regulators could then serve as the basis of the next generation of diagnostics and therapeutics in this devastating disease.

## METHODS

The data that support the findings of this study are available from the corresponding authors upon reasonable request.

### Pulmonary Arterial Endothelial Cell Culture

Human pulmonary artery endothelial cells (PAECs; Lonza, CC-2530) were cultured in endothelial cell growth basic medium-2 (Lonza, CC-3121) supplemented with growth factors (Lonza, CC-3202). PAECs are characterized by positive immunofluorescent staining for von Willebrand factor antigen and CD31/PECAM-1 (platelet endothelial cell adhesion molecule-1). Cell lines tested negative for HIV, hepatitis B, hepatitis C, and mycoplasma. Human PAECs at passage 5 to

10 were used for the experiments. Our laboratory performs intermittent testing for mycoplasma and had no positive results when this work was performed. All cells were maintained in a humidified chamber at 37 °C and 5% CO<sub>2</sub>. For IL-1 $\beta$  (interleukin-1 beta) experiments, cells were treated with recombinant human IL-1 $\beta$  (10ng/mL, PeproTech) at 70% to 80% confluency for 48 hours in complete endothelial cell media with vehicle control in DMSO. For hypoxia exposure experiments, cells were plated in 6-well cell culture plates at 1 $\times$ 10<sup>5</sup> cells per well, grown for 24 hours, and placed into a normobaric hypoxia chamber (1% O<sub>2</sub>) for 24 hours.

### Pulmonary Artery Smooth Muscle Cell Experiments

Early-passage (3–8 passage) human pulmonary artery smooth muscle cells isolated from small (<1 mm outer diameter) pulmonary arteries of patients with PAH and nondiseased subjects were provided by University of California Davis Lung Center Pulmonary Vascular Disease Program human specimens biobank, University of Pittsburgh Vascular Medicine Institute Cell Processing Core under approved protocols in accordance with institutional review board and Committee for Oversight of Research and Clinical Training Involving Decedents policies (institutional review board protocol and exempt #PRO14010265 and #PRO13050218). Cell isolation, characterization, and maintenance were performed under Pulmonary Hypertension Breakthrough Initiative-approved protocols, as described previously.<sup>28–31</sup> Cells were maintained in complete PromoCell Smooth Muscle Cell Growth Medium 2 with SupplementPack and Antibiotic-Antimycotic. Before experiments, cells were incubated for 48 hours in basal media supplemented with 0.1% BSA (for immunoblot lysates) or with 0.2% FBS (for RNA isolation).

### Transfection

Human PAECs were transfected at ~70% confluency in Opti-MEM media (Thermo Fisher Scientific) with 30 nmol/L negative control (Catalog#: 4390844), ACTN4 (s959), HLA-DPA (s226278), or CLDN1 (claudin-1; s17316) silencer select siRNA (Thermo Fisher Scientific) using Lipofectamine 2000 (Life Technologies), according to the manufacturer's instructions (Thermo Fisher Scientific). After 8 hours, Opti-MEM media was replaced by endothelial growth media, and cells were analyzed or used for subsequent experiments 48 hours after transfection.

### RNA Isolation, Reverse Transcription, and Quantitative Real-Time Polymerase Chain Reaction

Total RNA from cells and lung tissues was isolated using QIAzol reagent (Qiagen) according to the



manufacturer's protocol, and 0.5  $\mu\text{g}$  (for mRNA measurement) of total RNA was reverse transcribed into cDNA using high-capacity cDNA reverse transcription kit (Thermo Fisher Scientific). Quantitative real-time polymerase chain reactions (PCRs) were performed on a QuantStudio Flex Real-time PCR system (Applied Biosystems) with ACTN4 (Hs00245168\_m1), HLA-DPA1 (Hs01072899\_m1), CLDN1 (Hs00221623\_m1), and HLA-DPB1 (Hs03045105\_m1) TaqMan primers (Thermo Fisher Scientific). For mRNA control, the housekeeping gene  $\beta$ -actin (Hs01060665\_g1) TaqMan primers (Thermo Fisher Scientific) were used. The results were calculated using the  $2^{-\Delta\Delta\text{CT}}$  method.

### Immunoblotting

Protein was prepared by lysing cells in RIPA buffer (Sigma) supplemented with protease inhibitor (Thermo Fisher Scientific). Then, 10 to 25  $\mu\text{g}$  of total lysates per lane were loaded on 10% or 12% SDS-PAGE and transferred onto polyvinylidene difluoride membranes (Bio-Rad). The membranes were blocked with 5% skim milk dissolved in Tween-20/phosphate-buffered saline for 1 hour at room temperature. The membranes were probed with primary antibodies against ACTN4 (IgG, 1:1000, Thermo Fisher Scientific, H0000081-M01) and HLA-DPA1 (IgG, 1:500, Thermo Fisher Scientific, PA5-28037), overnight at 4  $^{\circ}\text{C}$ . Samples were normalized to  $\beta$ -actin (IgG, 1:1000, Invitrogen, AC-15) or PARP1 (poly(ADP-ribose) polymerase 1) (IgG, 1:1000, Thermo Fisher Scientific, PA5-16452). Protein bands were visualized, and digitized images were quantified using Image Lab software (Bio-Rad). Immunoblots and quantitative results are representative of at least 3 individual experiments. Antibodies were validated via siRNA-mediated knockdown or lentivirus-mediated overexpression experiments in PAECs and subsequent comparison of immunoblot results with control samples.

### Mass Spectrometry

SNP-specific DNA competition pulldown-mass spectrometry<sup>25</sup>. In brief,  $\sim 15\mu\text{g}$  of the purified SNP-specific DNA competition pulldown construct DNA was conjugated to 150  $\mu\text{L}$  Dynabeads™ M-280 Streptavidin (Life Technologies) according to the manufacturer's instruction. The DNA beads were then washed and mixed with 1 mg nuclear protein extracts in a buffer containing 40-fold excess of 7d competitor (a negative competitor that has the same fSNP sequence but contains a 3bp deletion on both sides of the SNP site, including the SNP) at room temperature for 1 hour. After separation and washing, the protein-DNA beads were digested with 5  $\mu\text{L}$  *EcoRI* (100 units/ $\mu\text{L}$ , New England Biolabs) at 37  $^{\circ}\text{C}$  for 30 minutes to remove the 3' DNA plus the proteins that bound to this non-SNP region. After separation and

washing, the protein-DNA beads were subsequently digested with 5  $\mu\text{L}$  *BamHI* (100 units/ $\mu\text{L}$ , New England Biolabs) at 37  $^{\circ}\text{C}$  for 45 minutes to release the fSNP sequence plus the fSNP-bound proteins. The supernatant was run on an 8% short SDS-PAGE gel and then collected for protein complex identification by mass spectrometry. For mass spectrometry analysis, 2 technical replicates were performed in parallel for each SNP.

### Electrophoretic Mobility Shift Assay

Electrophoretic mobility shift assay was performed using the LightShift Chemiluminescent EMSA Kit (Thermo Fisher Scientific) according to the manufacturer's instructions. For the probe, a 31 bp SNP fragment with the SNP centered in the middle was made by annealing 2 oligos. The double-stranded oligos were then biotinylated using the Biotin 3' End DNA Labeling Kit (Thermo Fisher Scientific). Nuclear extract from human arterial endothelial cells was isolated using NE-PER Nuclear and Cytoplasmic Extraction Reagents (Thermo Fisher Scientific) according to the manufacturer's instructions.

### Allele-Imbalanced DNA Pulldown Western Blot

Allele-imbalanced DNA pulldown Western blot to detect allele specific binding of ACTN4 to SNP rs9277336 was performed as previously described.<sup>25</sup> In brief, a 31 bp biotinylated SNP sequence centered with either A or G allele of SNP rs9277336 was generated by annealing 2 biotinylated primers (Integrated DNA Technologies). Approximately 1  $\mu\text{g}$  DNA was then attached to 40  $\mu\text{L}$  of Dynabeads™ M-280 Streptavidin. DNA beads were mixed with  $\sim 100\mu\text{g}$  of nuclear protein extracts isolated from human PAECs at room temperature for 1 hour with rotation. After washing off the unbound proteins, the DNA bound proteins were eluted by sample buffer and resolved on an SDS-PAGE gel for Western blot analysis using an antibody directed against ACTN4. For an internal control, the same blot was probed using an antibody directed against PARP1.

### Luciferase Reporter Assay

Luciferase reporter assays were performed in 293T cells using luciferase reporter vector pGL3-Promoter vector (Catalog #: E1761, Promega). The 35 bp SNP rs9277336 fragments were cloned into *Sac I* and *Xho I* sites in pGL3-Promoter vector individually. For control, an irrelevant 35bp fragment was cloned into the same vector. Both the sample construct and the control construct were transfected into 293T cells by FuGENE HD transfection reagent (Promega) together with the same amount of the vector pRL-TK that provides constitutive expression of *Renilla* luciferase (Catalog #: E2241,

Promega). The firefly luciferase reporter activity was measured by normalizing the firefly luciferase reporter activity to the *Renilla* luciferase activity using the Dual-Glo® Luciferase Reporter Assay System (Promega). All experiments were performed according to the manufacturer's protocol. The data represent 8 independent biological replicates (n=8).

## Hospitalization Analysis in the *All of Us* Cohort

The *All of Us*<sup>32</sup> (data set v6) platform was queried for patients with a diagnosis of PAH (concept identifier 4013643) and genomic sequencing by genotyping array (N=679 participants). One hundred and thirty-three individuals with missing demographic data (age, sex, or race) were excluded from the analysis (final n = 546 participants). All subjects gave informed consent for the *All of Us* study. Select demographic data are included in [Table S1](#). Hospitalizations were counted from all associated visit occurrences labeled as “inpatient encounter” (concept identifier 9201) or “ER or inpatient encounter” (concept identifier 262). Genetic association with the outcome of total hospitalizations was analyzed using a zero-inflated negative binomial model adjusted for age, race, and sex with an offset of years from diagnosis to the earlier of death or the end date of the curated data repository (January 1, 2022). *P* values and 95% CI were calculated using Huber robust sandwich variance estimator.<sup>33</sup> Analyses were performed using the *ZeroInflatedNegativeBinomialP* function of *statsmodels* v0.13.5 in Python 3.7.12.<sup>34</sup> Code is available upon request to *All of Us* users with access to the controlled tier data set. We considered adjusted  $P < 0.05$  as statistically significant.

## Human Cohorts, Samples, and Approvals

Self-identified European-descent patients with PAH were recruited into a biobank and registry at the University of Pittsburgh Medical Center (UPMC) Pulmonary Hypertension Comprehensive Care Center (Pittsburgh, PA) between 2016 and 2021. A total of 84 patients were enrolled who were diagnosed with World Symposium on Pulmonary Hypertension Group 1 PAH and where DNA was available for SNP genotyping. All subjects gave informed consent. These included predominantly idiopathic PAH along with hereditary PAH, congenital heart disease-associated PAH, and toxin-associated PAH ([Table S2](#)). Diagnosis was made by an expert physician, based on recent World Symposium on Pulmonary Hypertension criteria of having an elevated mean pulmonary arterial pressure >20 mmHg, pulmonary capillary wedge pressure ≤15 mmHg, and pulmonary vascular resistance ≥3 Wood units by right heart catheterization.<sup>35</sup> The expert physician adjudicated the diagnosis by ruling out

connective tissue disease, left heart disease, hypoxic lung disease, or chronic thromboembolic disease as primary drivers of PAH. Lung samples from human patients with PAH and nondiseased patients were used for immunofluorescent staining and whole lung homogenate experiments. The number of recruited patients was determined by availability of clinical samples. Experimental procedures were approved by the University of Pittsburgh Institutional Review Board (STUDY19050364, University of Pittsburgh). Ethical approval and informed consent conformed to the standards of the Declaration of Helsinki.

## SNP Association Analysis/Linear Regression

Genomic DNA was isolated from blood using either Puregene or QIAamp DNA isolation kit (Qiagen NV, Venlo, the Netherlands). SNP rs9277336 A and G alleles were identified using TaqMan platform with custom designed primer and probes (Thermo Fisher Scientific, Catalog ID: 4332073; [Table S3](#)). Quantitative real-time PCR reactions were performed on a QuantStudio Flex Real-time PCR system. To test the effect of SNP on markers of PAH, we applied multiple linear regression to adjust for age, sex, and vasodilator treatment. Confounders were selected based on preexisting knowledge. Specifically, a dominant genetic model was applied to test the association between each parameter assessed on right heart catheterization and SNP rs9277336. Three models for this analysis were developed, including unadjusted, adjusted for sex, and fully adjusted for age, sex, and vasodilator treatment. In each model, the effect of SNP on each trait was reported as coefficient (95% CI and *P* value). *P* values and 95% CI were calculated using Huber robust sandwich variance estimator.<sup>33</sup> We considered adjusted  $P < 0.05$  as statistically significant.

## RNA Sequencing

Total RNA was collected from 3 biological replicates of human PAECs treated with siRNA targeting ACTN4 (30 nmol/L), HLA-DPA1 (30 nmol/L), or negative control (30 nmol/L). Broad range RNA Qubit quality control and long RNA sequencing (paired-end read 75 cycles, 40–50 M reads/sample) was run by the University of Pittsburgh Health Sciences Sequencing Core. Transcript quantification was performed using Salmon and differential expression using DESEQ.<sup>36,37</sup> Pathway enrichment of direct Gene Ontology biological processes was performed using DAVID version 6.8 on genes with an absolute log fold change >1.2 and false discovery rate corrected *P* value <0.05.<sup>38–40</sup> The RNA sequencing data generated in this study have been deposited on the National Center for Biotechnology Information GEO Repository (accession number: GSE221290).

## Animal Models

All experiments were performed under protocols approved by the University of Pittsburgh Institutional Animal Care and Use Committee. For the monocrotaline PH rat model, as previously described,<sup>27</sup> male Sprague–Dawley rats (10–14 weeks old) procured from Charles River Laboratories (Wilmington, MA) were injected (intraperitoneally) with monocrotaline (60 mg/kg) versus PBS and kept for 26 days in normoxia (n=6 per group). The number of animals in each group was calculated to measure at least a 20% difference between means of experimental and control groups with a power of 80% with an SD of 20%. Following euthanasia, Tissue-Tek OCT (VWR) tissue preparation for histologic staining was done, as previously described.<sup>27</sup> Randomization of the animals assigned to different experimental groups was achieved. Briefly, populations of animals sharing the same sex, same genotype, and similar body weight were generated and placed in 1 container. Then, each animal was picked randomly and assigned in a logical fashion to different groups. For example, the first one is assigned to group A, second to group B, third to group A, fourth to group B, and so forth. No animals were excluded from analyses.

## Immunofluorescence

Cryostat sections of 5 to 7  $\mu\text{m}$  from OCT-embedded lung tissues were mounted on gelatin-coated histological slides (Thermo Fisher Scientific). Sections were blocked with 5% donkey serum and 2% BSA in PBS for 1 hour at room temperature. Primary antibodies were diluted in 2% BSA and incubated at 4  $^{\circ}\text{C}$  overnight. Small pulmonary vessels (30–100  $\mu\text{m}$  diameter) present in a given tissue section that were not associated with bronchial airways were selected for analysis. Intensity of staining was quantified using ImageJ software (National Institutes of Health). Analyses were performed blinded to condition as previously described by our group and collaborators.<sup>41–43</sup>

## Tube Formation Assay

Capillary tube formation assay was performed using a Cultrex In Vitro Angiogenesis Assay Kit (R&D Systems). Briefly, 50  $\mu\text{L}$  Matrigel containing reduced growth factors were added per well to 96-well plates that were polymerized for 30 minutes at 37  $^{\circ}\text{C}$ . Human PAECs pretreated with siRNA for 2 days (described previously) were then added at  $2 \times 10^4$  cells per well. Brightfield images were taken after 6 hours (EVOS XL Core Imaging System) with 20 $\times$  magnification. The number of branch joint points was quantified by a blinded observer in triplicate determinations from 3 separate experiments.

## Lentivirus Packaging

Human cDNA of ACTN4 was amplified by PCR, cloned into the lentiviral vector pCDH-CMV-MCS-EF1-copGFP (System Bioscience), and confirmed by DNA sequencing. HEK293FT cells were grown in DMEM containing 10% FBS and transfected using Lipofectamine 2000 (Life Technologies) with lentiviral plasmids along with a packaging plasmid system (LV-MAX<sup>TM</sup> Lentiviral Packaging Mix, Thermo Fisher Scientific), according to the manufacturer's instructions. Viral particles were harvested 48 to 60 hours after transfection, sterile filtered (0.45  $\mu\text{m}$ ), concentrated, and supplemented with 8  $\mu\text{g}/\text{mL}$  polybrene.

## Viral Transduction

PAECs were cultured in antibiotic-free endothelial cell growth basic medium-2 media to 60% confluency in 12-well plates and treated with or without 2 ng/mL IL-1 $\beta$  24 hours before transduction. Titered viral supernatant carrying the ACTN4 transgene (0.5 mL) was directly added to PAEC culture and incubated for 24 hours. The following day, 0.5 mL of endothelial cell growth basic medium-2 media was added and incubated for additional 24 hours. Commercially purchased CLDN1 lentivirus particles (Charles River, Catalog #LH894885) was used at a MOI 5 for CLDN1 overexpression experiments. Transduction was performed for 3 to 5 days and repeated as needed to achieve significant overexpression.

## IL-1 $\beta$ and IL-6 ELISA

ELISA assays were performed per manufacturer's instructions: 1L-1 $\beta$  (Abnova IL-1B Human ELISA Kit, Catalog # 89-100-305) and IL-6 (Abnova IL-6 Human ELISA Kit, Catalog # 89-333-244) using human plasma samples from the 84-patient UPMC cohort (Table S2).

## Statistical Analysis

All cell culture experiments presented in this study represent 3 independent experiments conducted in triplicate. Outcome of experiments in 2 groups was compared by 2-tailed permuted *t* test in Stata 17.0 (StataCorp 17.0, College Station, TX). For comparisons among multiple groups, we used package 'coin' version 1.4-2 in R to calculate the *P* value from permuted ANOVA using Monte Carlo Fisher-Pitman test. Bonferroni's post hoc analyses were performed. Data are represented as mean  $\pm$  SEM.

## RESULTS

### Eight Candidate SNPs Are in Linkage Disequilibrium with SNP rs2856830

Based on our post-GWAS functional genomics approach,<sup>25–27</sup> we first determined that SNP rs2856830



is in LD, or nonrandom association with 8 other SNPs as defined by  $r^2 > 0.80$  (Table 1). All associated SNPs were located within the 3' untranslated region, intronic region, or within 2.2 kB of the HLA-DPA1 locus on chromosome 6 (Figure 1A). Oligonucleotides containing the major and minor alleles of the original SNP and SNPs in LD were exposed to nuclear protein extract from human PAECs and subjected to electrophoretic mobility shift assays (Figure 1B, Figure S1). Endothelial cells were chosen because of the previously described correlation of endothelial expression of major histocompatibility complex Class II genes, including the HLA-DP family, with diffuse endothelial dysfunction seen in various autoimmune conditions.<sup>44,45</sup> The tag SNP rs2856830 displayed negligible difference in binding between the 2 alleles. In contrast, of the 8 SNPs in LD, 3 (rs9277334, rs9277336, rs2071362) showed differential protein binding between the 2 respective oligonucleotides. Using SNP-specific DNA competition pulldown-mass spectrometry, protein lysate bound to major allele oligonucleotides of these 3 SNPs was submitted for mass spectrometry analysis. Analysis of SNP rs9277336 revealed the greatest number of nuclear binding partners and was subsequently chosen for further analysis as a candidate fSNP relevant to the original associations of SNP rs2856830 to PAH (Table 2).

### SNP rs9277336 Is Associated With Improved Cardiac Output and Hospitalization Frequency in PAH

SNP rs9277336 (G>A) is present on chromosome 6 (chr6:33063108) with a mean alternate allele frequency of 0.132 to 0.272 depending on the study and population of interest, with a greater prevalence in African and South Asian populations.<sup>46</sup> Based on these findings and the close LD relationship with rs2856830, we sought to determine whether SNP rs9277336 carries independent associations to severity of PAH. To investigate, we compared hospitalizations as a marker of PAH severity in the *All of Us* database.<sup>32</sup> Among participants carrying a diagnosis of PAH, those having G/A or A/A versus G/G genotypes at rs9277336 (dominant genetic model) had significantly fewer hospitalizations in a zero-inflated negative binomial model offset for time since diagnosis and adjusted for age, sex, and race (Figure 1C). We then compared these results to a cohort with PAH recruited at UPMC. Genomic DNA was isolated from peripheral blood mononuclear cells of 84 patients with PAH and genotyped for presence of G (major) or A (minor) alleles (Figure 1D, Table S2). To assess association with disease severity, clinically relevant parameters of cardiovascular and pulmonary function were additionally compared with SNP genotype. After controlling for age, sex, and vasodilator

treatment status via dominant genetic modeling, Fick cardiac output and Fick cardiac index, markers of clinical severity and prognosis,<sup>47,48</sup> were found to be increased in patients with G/A or A/A genotypes compared with G/G genotypes (Figure 1E). Taken together, consistent with the association of the minor allele of the originally identified tag SNP rs2856830 with PAH improved survival,<sup>15</sup> we found that SNP rs9277336 A allele is associated with improvement in markers of disease severity, including cardiac output in PAH.

### SNP rs9277336 Differentially Binds Nuclear Alpha Actinin 4 Protein

Mass spectrometry proteomics of protein lysate bound to SNP rs9277336 G allele revealed 11 binding proteins (Table 2). ACTN4 displayed the greatest spectral counts. ACTN4 is an actin binding protein with known endothelial functions,<sup>49,50</sup> involved in cytoskeleton organization, regulation of nuclear transcription factor activity, and virus replication<sup>51</sup> but not implicated previously in PAH. To determine whether ACTN4 differentially binds to SNP rs9277336 alleles, allele-imbalanced DNA pulldown Western blot was performed, via a process by which biotinylated oligonucleotides containing the G and A alleles were combined with human PAEC nuclear protein and bound protein was isolated by streptavidin pulldown.<sup>25</sup> ACTN4 was bound more to the A allele compared with the G allele (Figure 1F). We sought to compare the functionality of the SNP A versus G allele in transcriptional activation by comparing luciferase reporter plasmids that carried the A versus G allele of SNP rs9277336 upstream of the reporter gene. Consistent with the biochemical data in Figure 1F, after transfection into HEK293 cells, luciferase activity with the plasmid carrying the A allele was higher than that of the G allele (Figure 1G). Taken together, these data indicate that SNP rs9277336 A allele binds more ACTN4 protein with resulting increase in transcriptional activity.

### PAH Triggers Decreased ACTN4 and HLA-DPA1 Expression In Vitro and In Vivo

Beyond the genetic association of ACTN4 and HLA-DPA1 with PAH, we next sought to determine if these genes are regulated in PAH by external triggers. We first assessed whether ACTN4 and HLA-DPA1 are regulated by acquired PAH stimuli independent of alterations of SNP rs9277336 genotype. The inflammatory cytokine and known PAH trigger, IL-1 $\beta$ ,<sup>52</sup> significantly decreased both ACTN4 and HLA-DPA1 expression in PAECs (Figure 2A and 2B). Other PH triggers, including hypoxia and oxidative stress, decreased HLA-DPA1 expression but had no effect on ACTN4 expression (Figure S2A and S2B). Together, these data

**Table 1. Eight SNPs Are in Linkage Disequilibrium With SNP rs2856830 Identified in Rhodes et al GWAS study<sup>15</sup>**

Variant	Pos (hg38)	LD (r <sup>2</sup> )	Major allele	Minor allele	African freq	American freq	Asian freq	European freq	Functional annotation
rs2856830	33073957	1	T	C	0.1	0.09	0.19	0.12	HLA-DPA1 Intron
rs9277334	33062335	0.9	A	C	0.27	0.12	0.19	0.12	2.2 kb from 3' of HLA-DPA1
rs9277336	33063108	0.87	G	A	0.27	0.12	0.2	0.12	1.5 kb from 3' of HLA-DPA1
rs9277338	33064586	0.82	T	A	0.04	0.09	0.19	0.11	HLA-DPA1 3' UTR
rs8807	33065074	0.9	T	C	0.26	0.12	0.19	0.12	HLA-DPA1 3' UTR
rs2071362	33065497	0.9	T	C	0.27	0.12	0.19	0.12	HLA-DPA1 Intron
rs2301226	33066819	0.87	G	A	0.26	0.11	0.19	0.13	HLA-DPA1 Intron
rs3830065	33069422	0.93	G	C	0.26	0.11	0.19	0.12	HLA-DPA1 Intron
rs2071349	33075743	0.96	C	G	0.13	0.1	0.19	0.12	HLA-DPA1 Intron

Eight SNPs are in LD, defined as r<sup>2</sup>>0.80, with SNP rs2856830. All SNPs are neighboring or located within the HLA-DPA1 gene locus located on chromosome 6. GWAS, indicates genome-wide association study; HLA, human leukocyte antigen; LD, linkage disequilibrium; SNP, single nucleotide polymorphism; and UTR, untranslated region.

demonstrate that ACTN4 and HLA-DPA1 are corepressed in PAECs in an IL-1β-dependent pathway but that HLA-DPA1 is affected by several other pathways key to PAH.

To define the relevance of ACTN4 and HLA-DPA1 regulation in PAH, we sought to quantify expression levels in animal and human instances of PAH. We assessed vascular expression of ACTN4 in multiple in vivo models of PAH, including humans and monocrotaline-treated rats (Figure 2C and 2D). Immunofluorescent confocal microscopy of the pulmonary vasculature revealed a reduction in ACTN4, particularly in the CD31+ endothelium, for World Symposium on Pulmonary Hypertension Group 1 patients with PAH and for monocrotaline-exposed PAH rats. Similarly, immunofluorescent confocal microscopy revealed decreased HLA-DPA1 in the pulmonary vasculature endothelium (Figure 2E and 2F). We found no difference in ACTN4 or HLA-DPA1 expression in whole lung homogenate or pulmonary arterial smooth muscle cells isolated from control versus patients with PAH (Figure S3A through S3C, Table S4), further supporting our rationale to study ACTN4 and HLA-DPA1 in PAECs before other cell types. Taken together, our findings emphasize the clinical relevance of reduced ACTN4 and HLA-DPA1 in PAH, consistent with genetic findings of the SNP rs9277336 G allele binding less ACTN4 and associated with worsened cardiac output in PAH.

### ACTN4 Controls HLA-DPA1 Expression

Guided by the findings of allele-specific SNP rs9277336 binding of transcriptionally active ACTN4 and the inflammatory downregulation of both ACTN4 and HLA-DPA1 in PAH, we sought to determine if ACTN4 regulates the neighboring HLA-DPA1 gene. In PAECs, ACTN4 knockdown significantly reduced HLA-DPA1 expression (Figure 3A). Conversely, when cells were pretreated with IL-1β to reduce endogenous ACTN4, forced ACTN4 expression increased HLA-DPA1 transcript expression (Figure 3B). Notably, lentiviral forced overexpression of ACTN4 without IL-1β did not affect HLA-DPA1 transcript, suggesting baseline levels of ACTN4 may already be saturating. Taken together, we found that ACTN4 upregulates endothelial HLA-DPA1 expression.

### ACTN4 and HLA-DPA1 Control Genes Important in Immune and Cell Cycle/Cell Structure Pathways in PAECs

Given such an ACTN4-HLA-DPA1 regulatory axis, we wanted to determine the downstream interconnected activities of ACTN4 and HLA-DPA1 in PAECs. A transcriptional microarray analysis was pursued in human PAECs after siRNA knockdown of ACTN4 or HLA-DPA1 as compared with control (Table S5).



Among those genes displaying significant alterations and ranked by fold change, several of the top 15 most highly upregulated genes by effect size in the siACTN4 condition were also found in the top 15 genes in the siHLA-DPA1 condition, including CLDN1, IFIT1 (interferon induced protein with tetratricopeptide repeats 1), IFIT3 (interferon induced protein with tetratricopeptide repeats 3), and CLIC3 (chloride intracellular channel 3). Likewise, LDB2 (LIM domain binding 2) was found in the top 15 most downregulated genes in both groups (Figure 3C and 3D). The genes altered under ACTN4 and HLA-DPA1 were compared against genes with a known PH gene network, defined and validated previously<sup>53</sup> as a network of downstream PH-related effectors derived from literature search and molecular interaction database mining<sup>54</sup> (Figure S4A and S4B, Table S6). Pathway analysis revealed significant enrichment of immune/inflammatory pathway changes, including interferon signaling, RhoA (ras homolog family member A) signaling, and p38 MAPK (mitogen-activated protein kinase) signaling, all of which have been implicated in PAH. Several cell cycle and cell structure pathways were also altered by both ACTN4 and HLA-DPA1 knockdown, including senescence, p53 signaling, Hippo signaling, and apoptosis signaling, all of which are also known to be involved in PAH (Figure 3E).

### CLDN1 Is Upregulated Under PAH Conditions In Vitro and In Vivo

CLDN1 was the top-ranked gene upregulated by siACTN4. CLDN1 is a structural component of tight junctions and associated with altered cellular permeability and dysregulation of epithelial-mesenchymal transition.<sup>55,56</sup> By real-time PCR in PAECs, we found that both ACTN4 and HLA-DPA1 knockdown upregulated CLDN1 (Figure 3F). Furthermore, CLDN1 was significantly upregulated by IL-1 $\beta$ , the same PAH trigger that downregulates both ACTN4 and HLA-DPA1 (Figure 3G, Figure S5). Correspondingly, immunofluorescent confocal microscopy of the pulmonary vasculature revealed an increase in CLDN1 in CD31<sup>+</sup> endothelium for both human and rodent instances of PAH (Figure 3H and 3I). Together, these data suggest the downstream importance of CLDN1 in the pathogenic activities of the ACTN4-HLA-DPA1 axis in PAECs.

### ACTN4-HLA-DPA1-CLDN1 Axis Affects Angiogenesis Consistent With PAH

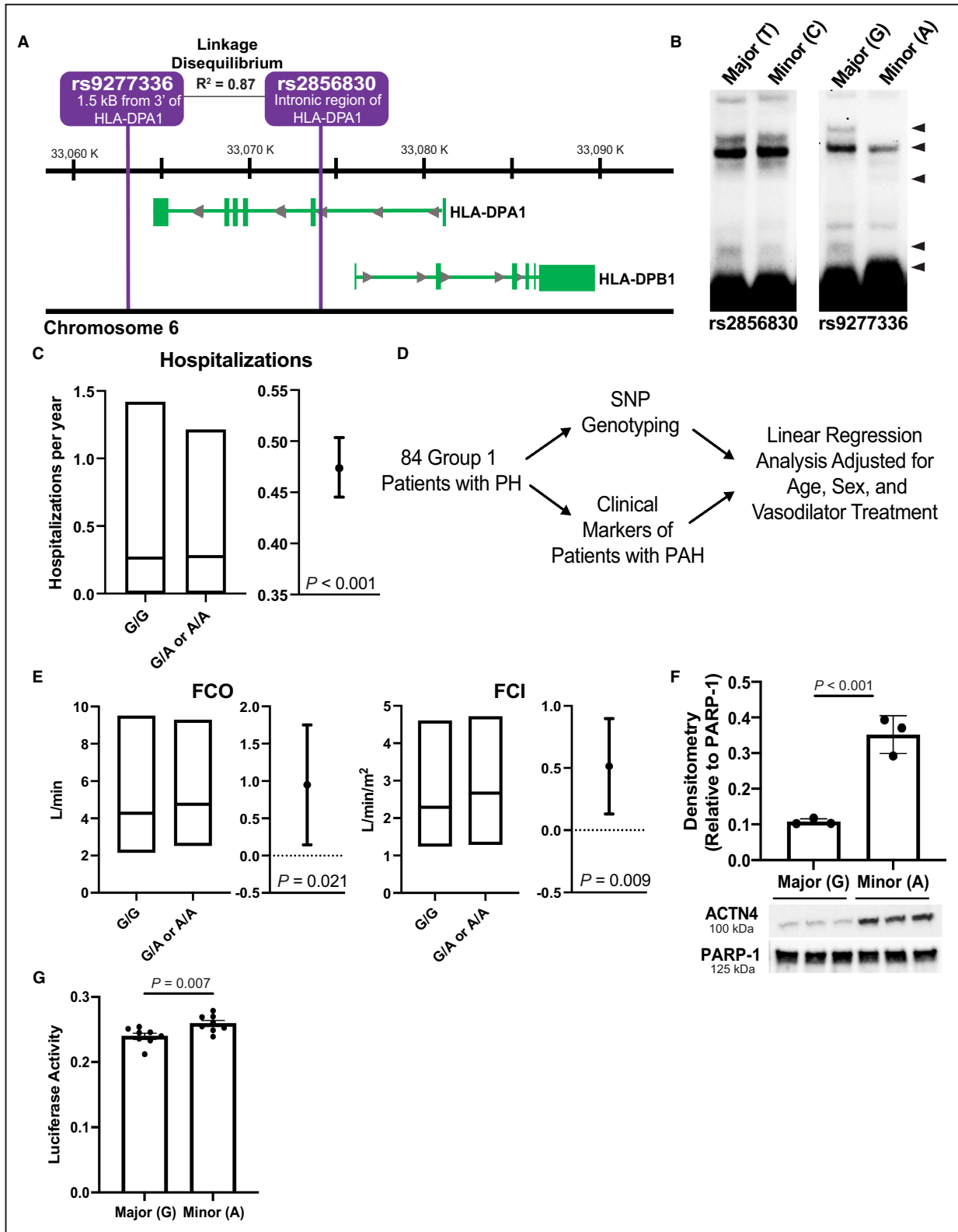
Finally, we assessed the role of ACTN4, HLA-DPA1, and CLDN1 in angiogenesis, an endothelial pathophenotype affected in PAH. Via in vitro tube formation assays, siRNA-mediated knockdown of ACTN4 and HLA-DPA1 inhibited angiogenesis (Figure 4A),

consistent with known endothelial pathophenotypes that drive PAH.<sup>57</sup> Conversely, lentivirus-mediated overexpression of ACTN4 increased angiogenic activity, including partial rescue of the reduced tube formation activity under IL-1 $\beta$ -mediated inflammatory conditions (Figure 4B). Lentivirus-mediated CLDN1 overexpression decreased angiogenesis, whereas CLDN1 knockdown increased angiogenesis. CLDN1 knockdown additionally rescued the reduced angiogenesis seen under IL-1 $\beta$  exposure (Figure 4C and 4D). Such pathophenotypes were consistent with reduced G allele-specific SNP rs9277336 binding to ACTN4 and the association to increased PAH disease severity. Thus, in total, our findings offer evidence that, either through genetic or inflammatory means, downregulation of the ACTN4-HLA-DPA1 regulatory axis drives endothelial dysfunction in PAH, in part mediated by CLDN1 expression.

## DISCUSSION

Several genomic variants have been associated to date with either risk or severity of PAH,<sup>58</sup> but the mechanisms underlying these associations, particularly those involving the common noncoding variants, are poorly understood.<sup>59</sup> In the case of the tag SNP rs2856830,<sup>60</sup> we investigated associated SNPs, determined functional capacity<sup>61</sup> of those SNPs, and identified differentially binding transcription factors. In doing so, we defined the pathogenic genomic architecture containing SNP rs9277336 including allele-specific binding of ACTN4 and identified targets that can drive PAH pathogenesis, explaining the association between this genetic locus and PAH outcomes<sup>62</sup> (Figure 5).

Bolstered by prior published success in other disease contexts, our post-GWAS approach to screen for allele-specific binding of transcription factors to linked SNPs offers an attractive direction for analyzing the underlying pathogenic mechanisms of other GWAS-identified SNPs in PAH and beyond. Future endeavors can be focused on other SNPs associated with PAH disease risk, such as those neighboring the *SOX17* locus.<sup>58</sup> Alternatively, noncoding SNPs surrounding the *IREB2* and *GALC* gene loci and associated with Group 3 PH have not been investigated for functionality.<sup>12</sup> Finally, because many of these putative fSNPs carry disparate mean allele frequencies across specific ethnic groups, such work may offer a viable process by which the mechanisms of race and ethnicity can be investigated as causative factors in PAH. For example, SNP rs9277336 A allele is more prevalent in individuals of African descent, perhaps providing a potential explanation for increased prevalence of pulmonary hypertension seen among Black Americans.<sup>63</sup> However, more extensive studies looking at the association of



this SNP with ethnicity and PAH presentation are indicated to better understand this possible link.

Our findings of the pathobiology of HLA-DPA1 also offer new insights to the molecular underpinnings of

disease severity in PAH. Inflammatory processes in PAH are appreciated as key contributing factors to pulmonary vascular remodeling, but questions remain as to whether inflammation and immune activation

**Figure 1. SNP rs9277336 allele differentially binds ACTN4 and is associated with worsened PAH severity.**

**A**, Schematic of SNPs rs2856630 and rs9277336. **B**, Electrophoretic mobility shift assay of human PAEC nuclear protein bound to oligonucleotides containing major (G/G) and minor alleles (G/A or A/A) of SNPs reveals differential protein binding between alleles of rs9277336, but not rs2856630. Black arrows represent differential binding proteins. **C**, Left panel shows median (IQR) of hospitalization rates of patients with PAH from the *All of Us* database by SNP rs9277336 genotype; right panel shows 95% CI adjusted for age, sex, and race. **D**, Schematic of Group 1 PAH in UPMC cohort and analysis of SNP genotype and clinical parameters of pulmonary hypertension. **E**, Left panel shows median (IQR) of Fick cardiac output and Fick cardiac index by SNP rs9277336 genotype of patients with PAH; right panel shows 95% CI of parameter adjusted for age, sex, and vasodilator treatment status. **F**, Pulldown assay of biotinylated oligonucleotides revealed differential binding of nuclear ACTN4 to rs9277336 A allele vs G allele. PARP-1 as loading control. n=3 in each group. **G**, Luciferase assay reveals increased transcription function with binding of ACTN4 to A allele. n=8 in each group. Data represented as mean±SEM or median with IQR. Significance determined by permuted *t* test or a robust sandwich variance estimator (C and E). ACTN4 indicates alpha actinin 4; FCI, Fick cardiac index; FCO, Fick cardiac output; HLA, human leukocyte antigen; IL-1 $\beta$ , interleukin-1 beta; IQR, interquartile range; PAEC, pulmonary arterial endothelial cell; PAH, pulmonary artery hypertension; PARP-1, poly(ADP-ribose) polymerase-1; SNP, single nucleotide polymorphism; and UPMC, University of Pittsburgh Medical Center.

are primary drivers of disease manifestation or progression.<sup>64</sup> In this study, we found that ACTN4 and HLA-DPA1 were downregulated by IL-1 $\beta$  treatment in PAECs, which mediated downstream endothelial dysfunction in angiogenic activity (Figure 4). Although immune and inflammatory pathways were implicated at the intracellular level in PAECs, our findings suggest that these pathways activate vascular endothelial pathophenotypes more readily than further release of soluble inflammatory markers into the circulating bloodstream. Correspondingly, when we assessed inflammatory cytokines IL-1 $\beta$  and IL-6 in plasma samples and neutrophil to lymphocyte ratios from our UPMC PAH cohort, no significant differences in those circulating markers were found, based on SNP genotype (Figure S6). Guided by our findings implicating the ACTN4-HLA-DPA1 axis in PAH severity, future studies will be poised to define better the mechanistic connections of diseases of autoimmunity and endothelial function, with intriguing connections to both pulmonary and peripheral vascular disease.

Our results additionally implicate ACTN4 in endothelial pathobiology and PAH pathogenesis. ACTN4 is an actin-binding protein involved in cytoskeleton organization, regulation of nuclear transcription factor activity, and virus replication.<sup>51</sup> Although our findings define the importance of SNP rs9277336 as at least 1 genomic site where ACTN4 exerts its pathogenic actions in PAH, it is likely that ACTN4 carries more pleiotropic transcriptional actions at other genomic loci. Consistent with the known parallels of cancer biology and PAH,<sup>65</sup> ACTN4 has been extensively studied in cancer, and its expression has been correlated with the aggressiveness, invasion, and metastasis in certain cancers such as nonsmall cell lung cancer, small cell lung cancer, and high-grade neuroendocrine lung tumors. Notably, patient tumors expressing higher levels of ACTN4 mRNA are clinically correlated to lower survival rates, diminished responses to certain chemotherapeutics, and higher recurrence rates following surgery.<sup>66</sup> Therapeutic approaches to decrease tumor expression of ACTN4 may be warranted, but given

our findings of the risk of PAH development with reduced ACTN4, such potential therapies should prioritize tissue-specific delivery or activity. Beyond PAH, consistent with the connection of HLA-DP genes with preeclampsia,<sup>23,24</sup> ACTN4 has also been implicated in preeclampsia, whereby decreased ACTN4 drives human umbilical vein endothelial cell dysfunction.<sup>49,67</sup> As such, future work could be envisioned to define further both the ACTN4-HLA-DPA1 axis and the functionality of SNP rs9277336 in preeclampsia.

In this report, we show several targets downstream of the ACTN4-HLA-DPA1 axis, most notably, including CLDN1. Claudins are key structural components of tight junctions and involved with intracellular signaling. In monocrotaline-exposed PAH rats, upregulation of CLDN1 in pulmonary arterial smooth muscle cells has been reported.<sup>68</sup> Similarly, CLDN1 was found to

**Table 2. Nuclear Human PAEC Protein ACTN4 Binds to SNP rs9277336**

Gene	Gene symbol	Spectral count	
		6	4
Alpha actinin 4	ACTN4	6	4
<i>Serine and arginine rich splicing factor 7</i>	<i>SRSF7</i>	2	1
<i>Serpin H member 1</i>	<i>SERPINH1</i>	5	1
<i>DNA topoisomerase II beta</i>	<i>TOP2B</i>	2	2
<i>Enhancer of rudimentary homolog</i>	<i>ERH</i>	2	2
<i>Retinoblastoma binding protein 6</i>	<i>RBBP6</i>	2	2
<i>Transformer 2 beta homolog</i>	<i>TRA2B</i>	2	1
<i>Serine and arginine rich splicing factor 9</i>	<i>SRSF9</i>	5	3
<i>Transcriptional factor A, mitochondrial</i>	<i>TFAM</i>	1	2
<i>Transcriptional activation suppressor family member 2</i>	<i>TASOR2</i>	1	1
<i>Pre-mRNA processing factor 19</i>	<i>PRP19</i>	1	1

Mass spectrometry revealed 11 nuclear PAEC proteins that are bound to the major allele. Protein binding represented by spectral count across independent experiments.

ACTN4 indicates alpha actinin 4; PAEC, pulmonary arterial endothelial cell; and SNP, single nucleotide polymorphism.

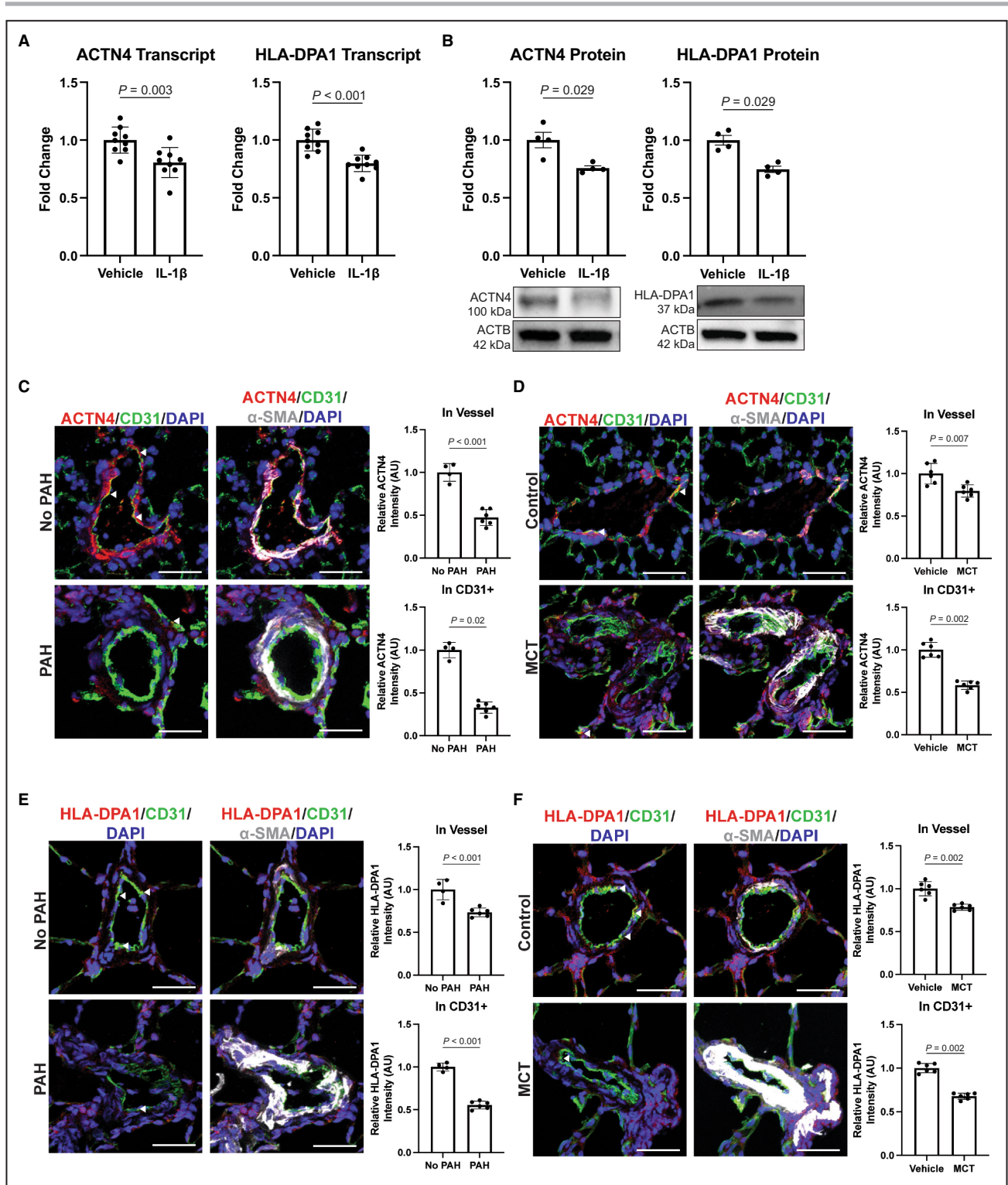


**Figure 2. ACTN4 and HLA-DPA1 levels are downregulated in vitro and in vivo PAH models.**

**A** and **B**, ACTN4 and HLA-DPA1 transcript expression under IL-1 $\beta$  treatment by RT-qPCR and immunoblotting. **C** and **D**, Representative images of Group 1 PAH and control human lungs and monocrotaline treated and control rats stained with immunofluorescent probes for ACTN4 (red), CD31 (green),  $\alpha$ -SMA (gray), nuclear counterstained with DAPI (blue), and imaged by confocal microscopy. White arrowheads depict colocalization of ACTN4 and CD31. Scale bar: 50  $\mu$ m. **E** and **F**, Representative images of Group 1 PAH and control human lungs and monocrotaline treated and control rats stained with immunofluorescent probes for HLA-DPA1 (red), CD31 (green),  $\alpha$ -SMA (gray), counterstained with DAPI (blue), and imaged by confocal microscopy. White arrowheads depict colocalization of HLA-DPA1 and CD31. Scale bar: 50  $\mu$ m. N=6 to 8 per group. Data represented as mean $\pm$ SEM. Significance determined by permuted *t* test.  $\alpha$ -SMA indicates alpha smooth muscle actin; ACTB, actin beta; ACTN4, alpha actinin 4; HLA, human leukocyte antigen; MCT, monocrotaline; PAH, pulmonary artery hypertension; and RT-qPCR, real-time quantitative polymerase chain reaction.



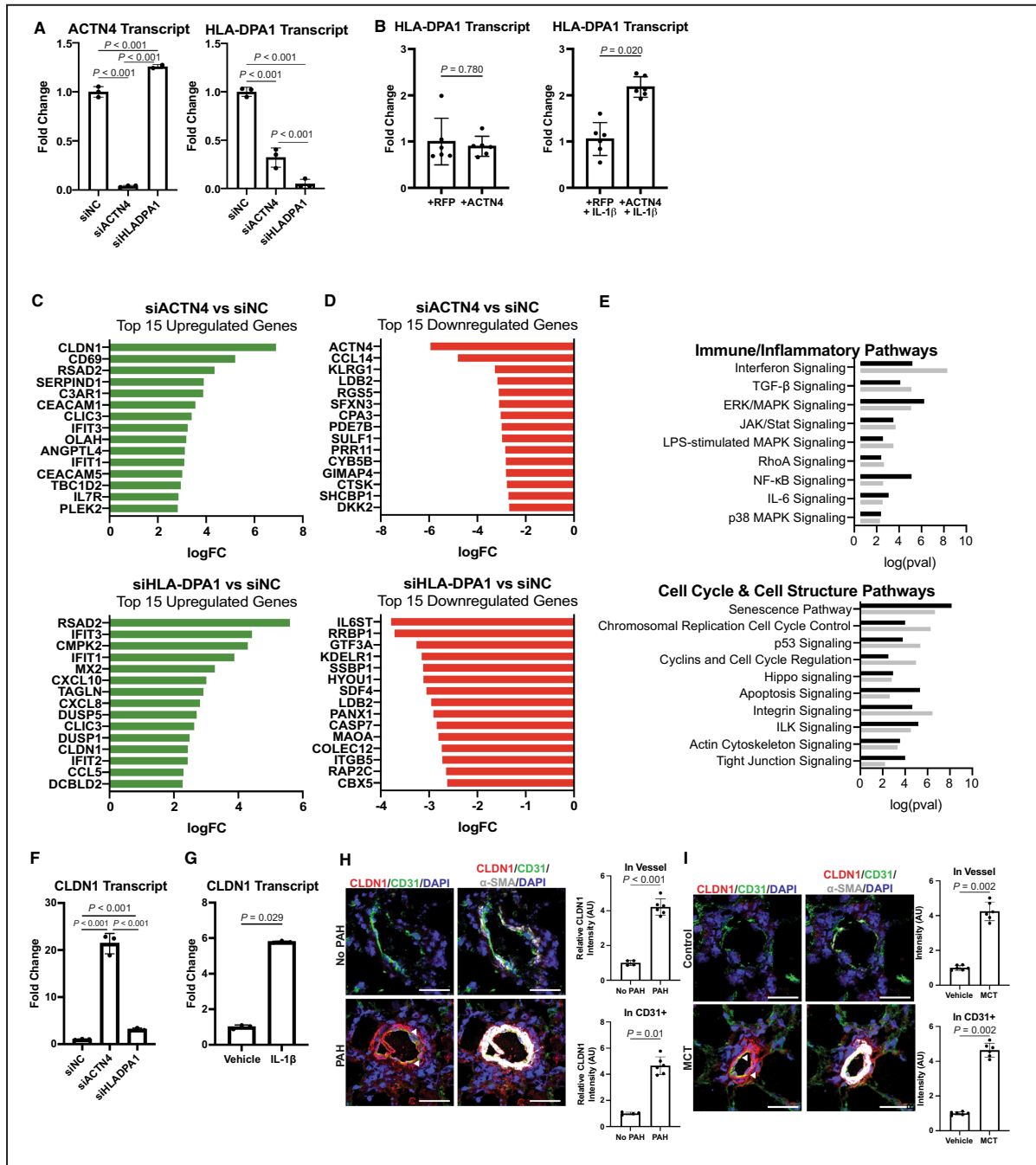


**Figure 3.** Transcriptional microarray of ACTN4 and HLA-DPA1 knockdown revealed gene expression and pathway changes.

**A**, ACTN4 and HLA-DPA1 transcript expression under siRNA-driven ACTN4 and HLA-DPA1 knockdown in PAECs. **B**, ACTN4 and HLA-DPA1 transcript expression under lentivirus forced overexpression of ACTN4 with and without pretreatment with IL-1 $\beta$  in PAECs. **C** and **D**, Top 15 upregulated and downregulated genes after ACTN4 and HLA-DPA1 knockdown in PAECs. **E**, Pathways enriched under siRNA mediated ACTN4 and HLA-DPA1 knockdown using Ingenuity Pathway Analysis software. n=3. **F**, CLDN1 transcript expression under siRNA mediated ACTN4 and HLA-DPA1 knockdown. **G**, CLDN1 transcript expression under IL-1 $\beta$  treatment. **H** and **I**, Representative images of Group 1 PAH and control human lungs and monocrotaline treated and control rats stained with immunofluorescent probes for CLDN1 (red), CD31 (green),  $\alpha$ -SMA (gray), nuclear counterstained with DAPI (blue), and imaged by confocal microscopy. Scale bar: 50  $\mu$ m. N=6 to 8 per group. Data represented as mean $\pm$ SEM. Significance determined by permuted *t* test or permuted ANOVA.  $\alpha$ -SMA indicates alpha smooth muscle actin; ACTN4, alpha actinin 4; CLDN-1, claudin-1; ERK, extracellular signal-regulated kinase; HLA, human leukocyte antigen; IL-1 $\beta$ , interleukin-1 $\beta$ ; IL-6, interleukin-6; ILK, integrin-linked kinase; JAK/STAT, Janus kinase/signal transducer and activator of transcription; LPS, lipopolysaccharide; MAPK, mitogen-activated protein kinase; NF- $\kappa$ B, nuclear factor kappa B; PAEC, pulmonary arterial endothelial cell; PAH, pulmonary artery hypertension; RFP, red fluorescent protein; RhoA, ras homolog family member A; and TGF- $\beta$ , transforming growth factor beta.



regulate pulmonary vascular remodeling through its effects on pulmonary artery smooth muscle cell proliferation. Additionally, SNPs in CLDN1 have been associated with various cancers and hepatitis susceptibility, seemingly because of their role in tight junction complexes.<sup>69–71</sup> However, to the best of our knowledge, SNPs in CLDN1 have not previously been implicated in pulmonary vascular disease.

The identification of the noncoding function of SNP rs9277336 in endothelial function may also be indicative of more complex genomic biology. Beyond the neighboring HLA-DPA1, the SNP's chromosomal position in relatively close proximity to HLA-DPB1 may suggest the role of this HLA-DP gene isoform in PAH.

Furthermore, the increasing fidelity of genomic mapping may suggest the importance of long-range chromatin interactions in the activity of this SNP. Namely, publicly available 3D-genome Interaction Viewer and database of high-throughput chromatin conformation capture have reported interactions of SNP rs9277336 across chromatin structure in silico.<sup>72</sup> Notably, these interactions appear to be independent of BMPR2 and other known rare pathogenic variants associated with PAH, but additional studies that include larger numbers of hereditary PAH cases would clarify whether rare pathogenic variants can contribute to the association of this SNP with PAH outcomes. Future studies should also be prioritized to characterize other putative

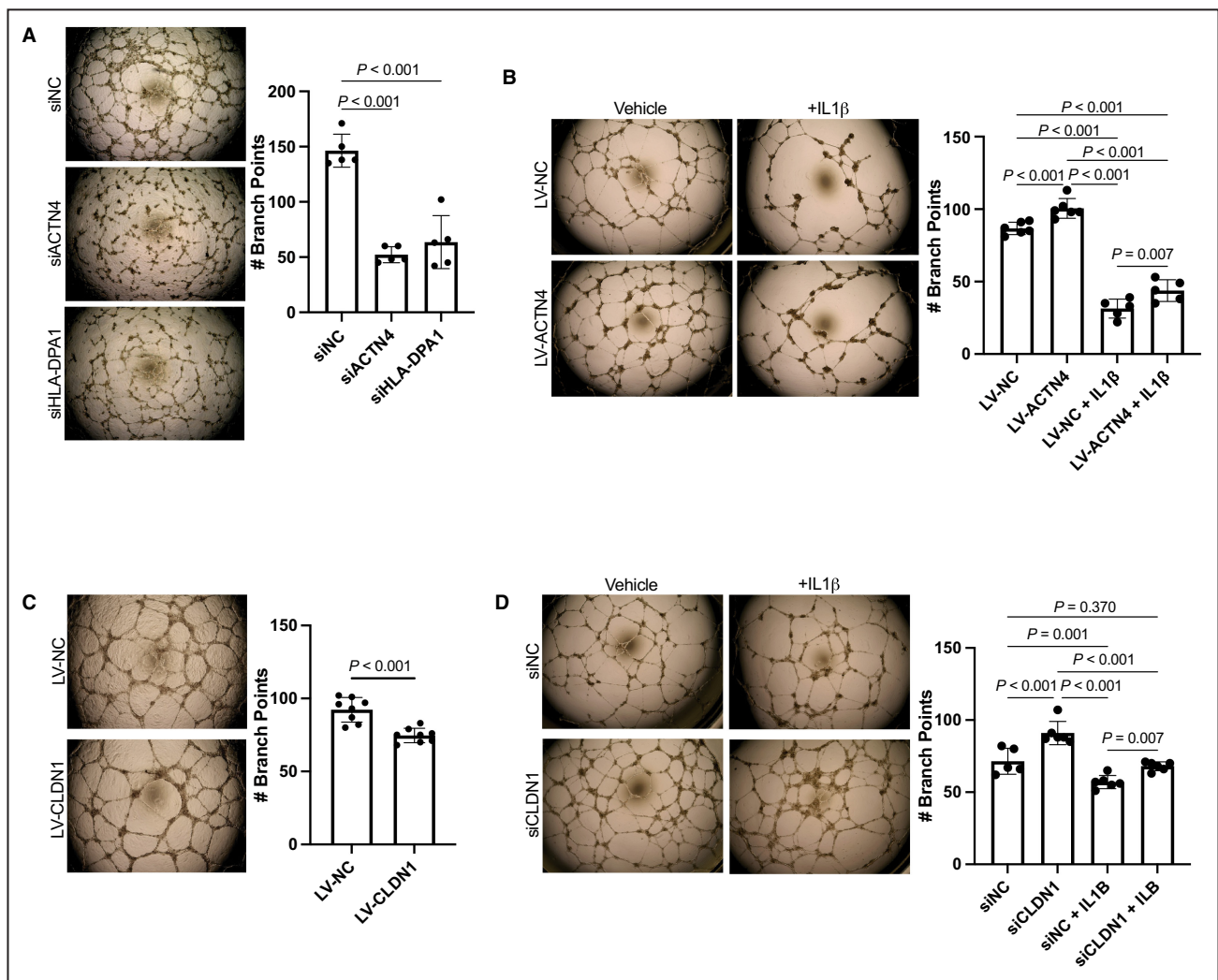


**Figure 4. ACTN4-HLA-DPA1-CLDN1 axis affects angiogenesis, an endothelial phenotype associated with PAH.** **A**, Tube formation assay after siACTN4, siHLA-DPA1, and siNC knockdown in PAECs. **B**, Tube formation assay after LV-ACTN4 and LV-NC overexpression in PAECs under vehicle and IL-1β treatment. **C**, Tube formation assay after LV-CLDN1 overexpression in PAECs. **D**, Tube formation assay after siCLDN1 under vehicle and IL-1β treatment. Scale bar: 500 μm. n=5 to 8 per group. Data are represented as mean±SEM. Significance determined by permuted *t* test or permuted ANOVA. ACTN4 indicates alpha actinin 4; CLDN-1, claudin-1; HLA, human leukocyte antigen; IL-1β, interleukin-1β; LV-ACTN4, lentivirus-mediated ACTN4; LV-CLDN1, lentivirus-mediated CLDN1; LV-NC, lentivirus negative control; PAEC, pulmonary arterial endothelial cell; PAH, pulmonary arterial hypertension; siACTN4, siRNA-mediated ACTN4; siCLDN1, CLDN1 knockdown; siHLA-DPA1, siRNA-mediated HLA-DPA1; and siNC, siRNA-mediated negative control.

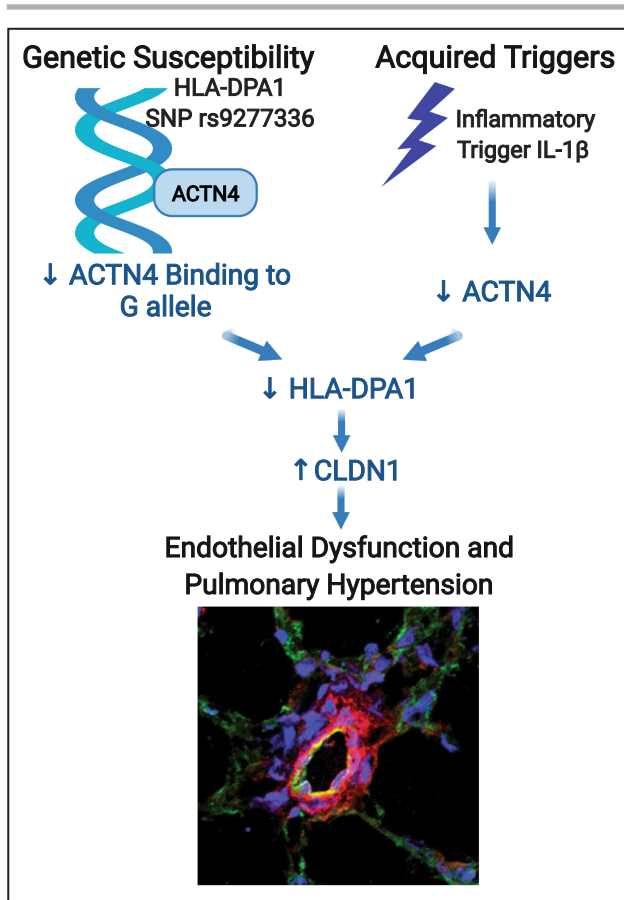


**Figure 5. Model of the rs9277336-ACTN4-HLA-DPA1 genomic axis in pulmonary arterial hypertension.**

In this study, we defined the pathogenic activity of functional SNP rs9277336, entailing the allele-specific binding of ACTN4, which controls expression of the neighboring HLA-DPA1 gene. Through inflammatory or genetic means, downregulation of this ACTN4-HLA-DPA1 regulatory axis promotes endothelial pathophenotypes, in part via CLDN1 expression, thus providing a mechanistic explanation for the association between this SNP and PAH outcomes. ACTN4 indicates alpha actinin 4; CLDN-1, claudin-1; HLA, human leukocyte antigen; IL-1 $\beta$ , interleukin-1 $\beta$ ; PAH, pulmonary arterial hypertension; and SNP, single nucleotide polymorphism.

long-range chromatin interactions for more extensive control of PAH manifestations.

There are limitations of this study. In vitro studies in this report were performed in cell lines containing only the SNP rs9277336 G/G genotype. Future studies are warranted to fully define the causative role of this SNP via its interaction with ACTN4, potentially using CRISPR-Cas9 genome editing at SNP rs9277336 to generate isogenic cells as we have reported.<sup>73</sup> Although major histocompatibility complex Class II genes and ACTN4's known expression and function in the endothelium guided our initial work, the ACTN4-HLA-DPA1 axis may also play pathogenic roles in other vascular cell types in PAH. Although we found no difference in ACTN4 and HLA-DPA1 expression in

whole lung homogenate or pulmonary artery smooth muscle cells isolated from patients with PAH and controls without PAH (Figure S3), additional investigation is warranted on the role of this axis in other cell types relevant to PAH. Furthermore, the putative causative role of this SNP in in vivo pathophysiology also was not explored here, as it is complicated by the nonconserved nature of SNP rs9277336 in rodents. The use of precision cut lung slices could be considered to compare human patients with PAH with differing SNP rs9277336 alleles, as has been described for nonconserved noncoding RNAs.<sup>74,75</sup> Alternatively, CRISPR-Cas9 technology could be applied to insert this human SNP directly into rodents near the HLA-DPA1 locus for downstream studies of PAH development.

In our PAH population studies, we also acknowledge limitations in sample size, particularly in the single-center patient cohort with PAH from UPMC. Additionally, we recognize that cardiac output and index as assessed by thermodilution have been correlated with mortality outcomes in patients with PAH.<sup>76,77</sup> However, in this single-center cohort where DNA genotyping was available, thermodilution measurements were not consistently reported. Thus, in addition to the significant association of SNP rs9277336 on estimated Fick cardiac output and index in this cohort with PAH (Figure 1E), future investigation encompassing larger patient cohorts will be necessary to elucidate whether thermodilution measures as well as other echocardiographic or hemodynamic measures of PAH and cardiac function are associated with this SNP. Finally, in regard to analyses of publicly available data from the National Institutes of Health-sponsored *All of Us* database, there are known limitations in the use of concept identifier codes alone for accurate and comprehensive identification of PAH.<sup>78,79</sup> Future work to incorporate objective indices or biomarkers of PAH (ie, pathognomonic imaging analyses or blood biomarker signatures) may increase confidence in the diagnostic accuracy of these concept identifier codes. Regardless, when coupled with the genomic and mechanistic data generated in this study, the association of hospitalization rate with SNP rs9277336 in PAH (Figure 1C) found in the *All of Us* database offers supportive evidence of the importance of this SNP in modulating PAH severity in human disease.

## CONCLUSIONS

In summary, we used a post-GWAS approach to define the mechanism underlying the association between a noncoding SNP and PAH outcomes. In endothelial cells, we demonstrated the allele-specific interaction of a fSNP rs9277336 with ACTN4 and induction of the neighboring HLA-DPA1, a process correlating

the rs9277336 G allele with worsened PAH severity. Furthermore, downregulation of this ACTN4-HLA-DPA1 regulatory axis was found to drive endothelial dysfunction, in part through CLDN1 expression, with direct relevance to PAH. Overall, these findings offer historically elusive mechanistic insight into the genomic and inflammatory processes underlying this mysterious disease.

## ARTICLE INFORMATION

Received August 22, 2022; accepted February 6, 2023.

### Affiliations

Center for Pulmonary Vascular Biology and Medicine, Pittsburgh Heart, Lung, and Blood Vascular Medicine Institute, Division of Cardiology, Department of Medicine, University of Pittsburgh School of Medicine and University of Pittsburgh Medical Center, Pittsburgh, PA (N.H., A.K., Y.Y., R.J.R., N.J.K., W.E.K., Y.A.A., Y.-Y.T., A.H., Y.T., D.M., W.S., S.Y.C.); School of Medicine, Tsinghua University, Beijing, China (Y.Y.); The Aging Institute, University of Pittsburgh School of Medicine, Pittsburgh, PA (D.J., T.W., G.L.); Division of Pulmonary Allergy and Critical Care Medicine, Department of Medicine, University of Pittsburgh Medical Center, Pittsburgh, PA (Y.Z., M.N.); Division of Pulmonary, Critical Care, and Sleep Medicine, Department of Internal Medicine, University of California Davis, Davis, CA (T.V.K., E.A.G., D.G.); and Université Côte d'Azur, CNRS, UMR7275, IPMC, Valbonne, France (T.B.).

### Acknowledgments

The *All of Us* Research Program is supported by the National Institutes of Health, Office of the Director: Regional Medical Centers: 1 OT2 OD026549; 1 OT2 OD026554; 1 OT2 OD026557; 1 OT2 OD026556; 1 OT2 OD026550; 1 OT2 OD026552; 1 OT2 OD026553; 1 OT2 OD026548; 1 OT2 OD026551; 1 OT2 OD026555; IAA #: AOD 16037; Federally Qualified Health Centers: HHSN 263201600085U; Data and Research Center: 5 U2C OD023196; Biobank: 1 U24 OD023121; The Participant Center: U24 OD023176; Participant Technology Systems Center: 1 U24 OD023163; Communications and Engagement: 3 OT2 OD023205; 3 OT2 OD023206; and Community Partners: 1 OT2 OD025277; 3 OT2 OD025315; 1 OT2 OD025337; 1 OT2 OD025276. In addition, the *All of Us* Research Program would not be possible without the partnership of its participants. We thank the University of Pittsburgh Health Sciences Sequencing Core for performing microarray and RNA sequencing. We thank the Center for Organ Recovery & Education, the organ donors, and their families for the human lung tissue samples presented in this study. Graphical abstract created with [BioRender.com](https://www.biorender.com).

### Sources of Funding

This study was supported by National Institutes of Health grants R01 HL124021 (S.Y.C.), R01 HL122596 (S.Y.C.), R01 HL150638 (E.A.G.), R01 HL13021 (E.A.G.), R01 HL113178 (E.A.G.), K08 HL 161435 (W.S.), T32 HL129964 (N.J.K.); American Heart Association grants 18EIA33900027 (S.Y.C.), CDA 857423 (W.S.); The McKamish Family Foundation, the Hemophilia Center of Western Pennsylvania, and the Institute for Transfusion Medicine (N.J.K.).

### Disclosures

Dr Chan has served as a consultant for Acceleron Pharma and United Therapeutics; has held research grants from Actelion, Bayer, United Therapeutics, and Pfizer; and is a director, officer, and shareholder of Synhale Therapeutics. Dr Chan and T. Bertero have filed patents regarding metabolic dysregulation in pulmonary hypertension. The other authors declare no competing interests.

### Supplemental Material

Tables S1–S6  
Figures S1–S6

## REFERENCES

- Rajagopal S, Yu Y-RA. The pathobiology of pulmonary arterial hypertension. *Cardiol Clin*. 2022;40:1–12. doi: [10.1016/j.ccl.2021.08.001](https://doi.org/10.1016/j.ccl.2021.08.001)
- Zeng Y, Li N, Zheng Z, Chen R, Liu W, Cheng J, Zhu J, Zeng M, Peng M, Hong C. Screening of key biomarkers and immune infiltration in pulmonary arterial hypertension via integrated bioinformatics analysis. *Bioengineered*. 2021;12:2576–2591. doi: [10.1080/21655979.2021.1936816](https://doi.org/10.1080/21655979.2021.1936816)
- Hon SM, Alpizar-Rivas RM, Farber HW. Pulmonary arterial hypertension in patients infected with the human immunodeficiency virus. *Cardiol Clin*. 2022;40:45–54. doi: [10.1016/j.ccl.2021.08.004](https://doi.org/10.1016/j.ccl.2021.08.004)
- Morrell NW, Aldred MA, Chung WK, Elliott CG, Nichols WC, Soubrier F, Trembath RC, Loyd JE. Genetics and genomics of pulmonary arterial hypertension. *Eur Respir J*. 2019;53:1801899. doi: [10.1183/13993003.01899-2018](https://doi.org/10.1183/13993003.01899-2018)
- Thenappan T, Ormiston ML, Ryan JJ, Archer SL. Pulmonary arterial hypertension: pathogenesis and clinical management. *BMJ*. 2018;360:j5492.
- Visscher PM, Yengo L, Cox NJ, Wray NR. Discovery and implications of polygenicity of common diseases. *Science*. 2021;373:1468–1473. doi: [10.1126/science.abi8206](https://doi.org/10.1126/science.abi8206)
- Zeng J, Xue A, Jiang L, Lloyd-Jones LR, Wu Y, Wang H, Zheng Z, Yengo L, Kemper KE, Goddard ME, et al. Widespread signatures of natural selection across human complex traits and functional genomic categories. *Nat Commun*. 2021;12:1164. doi: [10.1038/s41467-021-21446-3](https://doi.org/10.1038/s41467-021-21446-3)
- Zhang Y, Qi G, Park J-H, Chatterjee N. Estimation of complex effect-size distributions using summary-level statistics from genome-wide association studies across 32 complex traits. *Nat Genet*. 2018;50:1318–1326. doi: [10.1038/s41588-018-0193-x](https://doi.org/10.1038/s41588-018-0193-x)
- Holland D, Frei O, Desikan R, Fan C-C, Shadrin AA, Smeland OB, Sundar VS, Thompson P, Andreassen OA, Dale AM. Beyond SNP heritability: polygenicity and discoverability of phenotypes estimated with a univariate gaussian mixture model. *PLoS Genet*. 2020;16:e1008612. doi: [10.1371/journal.pgen.1008612](https://doi.org/10.1371/journal.pgen.1008612)
- Germain M, Eyries M, Montani D, Poirier O, Girerd B, Dorfmueller P, Coulet F, Nadaud S, Maugeen S, Guignabert C, et al. Genome-wide association analysis identifies a susceptibility locus for pulmonary arterial hypertension. *Nat Genet*. 2013;45:518–521. doi: [10.1038/ng.2581](https://doi.org/10.1038/ng.2581)
- Benza RL, Gomberg-Maitland M, Demarco T, Frost AE, Torbicki A, Langleben D, Pulido T, Correa-Jaque P, Passineau MJ, Wiener HW, et al. Endothelin-1 pathway polymorphisms and outcomes in pulmonary arterial hypertension. *Am J Respir Crit Care Med*. 2015;192:1345–1354. doi: [10.1164/rccm.201501-0196OC](https://doi.org/10.1164/rccm.201501-0196OC)
- Lee JH, Cho MH, Hersh CP, McDonald M-LN, Wells JM, Dransfield MT, Bowler RP, Lynch DA, Lomas DA, Crapo JD, et al. IREB2 and GALC are associated with pulmonary artery enlargement in chronic obstructive pulmonary disease. *Am J Respir Cell Mol Biol*. 2015;52:365–376. doi: [10.1165/rccb.2014-0210OC](https://doi.org/10.1165/rccb.2014-0210OC)
- Kimura M, Tamura Y, Guignabert C, Takei M, Kosaki K, Tanabe N, Tatsumi K, Saji T, Satoh T, Kataoka M, et al. A genome-wide association analysis identifies PDE1A|DNAJC10 locus on chromosome 2 associated with idiopathic pulmonary arterial hypertension in a Japanese population. *Oncotarget*. 2017;8:74917–74926. doi: [10.18632/oncotarget.20459](https://doi.org/10.18632/oncotarget.20459)
- Yin C, Li K, Yu Y, Huang H, Yu Y, Wang Z, Yan J, Pu Y, Li Z, Li D, et al. Genome-wide association study identifies loci and candidate genes for non-idiopathic pulmonary hypertension in eastern Chinese Han population. *BMC Pulm Med*. 2018;18:158. doi: [10.1186/s12890-018-0719-0](https://doi.org/10.1186/s12890-018-0719-0)
- Rhodes CJ, Batai K, Bleda M, Haimel M, Southgate L, Germain M, Pauciuolo MW, Hadinnapola C, Aman J, Girerd B, et al. Genetic determinants of risk in pulmonary arterial hypertension: international genome-wide association studies and meta-analysis. *Lancet Respir Med*. 2019;7:227–238. doi: [10.1016/S2213-2600\(18\)30409-0](https://doi.org/10.1016/S2213-2600(18)30409-0)
- Díaz-Peña R, Aransay AM, Bruges-Armas J, López-Vázquez A, Rodríguez-Ezpeleta N, Mendibil I, Sánchez A, Torre-Alonso JC, Bettencourt BF, Mulero J, et al. Fine mapping of a major histocompatibility complex in ankylosing spondylitis: association of the HLA-DPA1 and HLA-DPB1 regions. *Arthritis Rheum*. 2011;63:3305–3312. doi: [10.1002/art.30555](https://doi.org/10.1002/art.30555)
- Lantermann A, Hampe J, Kim WH, Winter TA, Kidd M, Nagy M, Fölsch UR, Schreiber S. Investigation of HLA-DPA1 genotypes as predictors of inflammatory bowel disease in the German, south African, and south Korean populations. *Int J Colorectal Dis*. 2002;17:238–244. doi: [10.1007/s00384-001-0382-3](https://doi.org/10.1007/s00384-001-0382-3)
- Alenzi MJ, Ghazy AA, Taha D-E. The weight of HLA-DPA1 rs3077 single nucleotide polymorphism in prostate cancer, a multi-center study. *Prostate Cancer*. 2021;2021:5539851–5539855. doi: [10.1155/2021/5539851](https://doi.org/10.1155/2021/5539851)



19. Hung Y-M, Cheng C-C, Wann S-R, Lin S-L. Ankylosing spondylitis associated with pulmonary arterial hypertension. *Intern Med.* 2015;54:431–434. doi: 10.2169/internalmedicine.54.3160
20. Malik TF, Aurelio DM. Extraintestinal manifestations of inflammatory bowel disease. *StatPearls.* Treasure Island, FL: StatPearls Publishing; 2022.
21. Werny L, Colmorgen C, Becker-Pauly C. Regulation of meprin metalloproteases in mucosal homeostasis. *Biochim Biophys Acta Mol Cell Res.* 2022;1869:119158. doi: 10.1016/j.bbamcr.2021.119158
22. Yang J, Wang F, Chen B. HLA-DPA1 gene is a potential predictor with prognostic values in multiple myeloma. *BMC Cancer.* 2020;20:915. doi: 10.1186/s12885-020-07393-0
23. Honda K, Takakuwa K, Hataya I, Yasuda M, Kurabayashi T, Tanaka K. HLA-DQB1 and HLA-DPB1 genotypes in severe preeclampsia. *Obstet Gynecol.* 2000;96:385–389.
24. Ooki I, Takakuwa K, Akashi M, Nonaka T, Yokoo T, Tanaka K. Studies on the compatibility of HLA-class II alleles in patient couples with severe pre-eclampsia using PCR-RFLP methods. *Am J Reprod Immunol.* 2008;60:75–84. doi: 10.1111/j.1600-0897.2008.00592.x
25. Zhao Y, Wu D, Jiang D, Zhang X, Wu T, Cui J, Qian M, Zhao J, Oesterreich S, Sun W, et al. A sequential methodology for the rapid identification and characterization of breast cancer-associated functional SNPs. *Nat Commun.* 2020;11:3340. doi: 10.1038/s41467-020-17159-8
26. Wu T, Jiang D, Zou M, Sun W, Wu D, Cui J, Huntress I, Peng X, Li G. Coupling high-throughput mapping with proteomics analysis delineates cis-regulatory elements at high resolution. *Nucleic Acids Res.* 2021;50:e5. doi: 10.1093/nar/gkab890
27. Zou M, Jiang D, Wu T, Zhang X, Zhao Y, Wu D, Sun W, Cui J, Moreland L, Li G. Post-GWAS functional studies reveal an RA-associated CD40-induced NF- $\kappa$ B signal transduction and transcriptional regulation network targeted by class II HDAC inhibitors. *Hum Mol Genet.* 2021;30:823–835. doi: 10.1093/hmg/ddab032
28. Jiang L, Goncharov DA, Shen Y, Lin D, Chang B, Pena A, DeLisser H, Goncharova EA, Kudryashova TV. Akt-dependent glycolysis-driven lipogenesis supports proliferation and survival of human pulmonary arterial smooth muscle cells in pulmonary hypertension. *Front Med (Lausanne).* 2022;9:886868. doi: 10.3389/fmed.2022.886868
29. Kudryashova TV, Dabral S, Nayakanti S, Ray A, Goncharov DA, Avolio T, Shen Y, Rode A, Pena A, Jiang L, et al. Noncanonical HIPPO/MST signaling via BUB3 and FOXO drives pulmonary vascular cell growth and survival. *Circ Res.* 2022;130:760–778. doi: 10.1161/CIRCRESAHA.121.319100
30. Kudryashova TV, Goncharov DA, Pena A, Kelly N, Vanderpool R, Baust J, Kobir A, Shufesky W, Mora AL, Morelli AE, et al. HIPPO-integrin-linked kinase cross-talk controls self-sustaining proliferation and survival in pulmonary hypertension. *Am J Respir Crit Care Med.* 2016;194:866–877. doi: 10.1164/rccm.201510-2003OC
31. Goncharov DA, Kudryashova TV, Ziai H, Ihida-Stansbury K, DeLisser H, Krymskaya VP, Tudor RM, Kawut SM, Goncharova EA. Mammalian target of rapamycin complex 2 (mTORC2) coordinates pulmonary artery smooth muscle cell metabolism, proliferation, and survival in pulmonary arterial hypertension. *Circulation.* 2014;129:864–874. doi: 10.1161/CIRCULATIONAHA.113.004581
32. Sankar PL, Parker LS. The precision medicine Initiative's all of us research program: an agenda for research on its ethical, legal, and social issues. *Genet Med.* 2017;19:743–750. doi: 10.1038/gim.2016.183
33. Freedman DA. On the so-called "Huber Sandwich Estimator" and "Robust Standard Errors". *Am Stat.* 2006;60:299–302. doi: 10.1198/000313006X152207
34. Seabold S, Perktold J. Statsmodels: econometric and statistical modeling with python. *Proceedings of the 9th Python in Science Conference.* Austin, Texas: SciPy; 2010:92–96.
35. Simonneau G, Montani D, Celermajer DS, Denton CP, Gatzoulis MA, Krowka M, Williams PG, Souza R. Haemodynamic definitions and updated clinical classification of pulmonary hypertension. *Eur Respir J.* 2019;53:1801913. doi: 10.1183/13993003.01913-2018
36. Patro R, Duggal G, Love MI, Irizarry RA, Kingsford C. Salmon provides fast and bias-aware quantification of transcript expression. *Nat Methods.* 2017;14:417–419. doi: 10.1038/nmeth.4197
37. Anders S, Huber W. Differential expression analysis for sequence count data. *Genome Biol.* 2010;11:R106. doi: 10.1186/gb-2010-11-10-r106
38. Huang DW, Sherman BT, Lempicki RA. Systematic and integrative analysis of large gene lists using DAVID bioinformatics resources. *Nat Protoc.* 2009;4:44–57. doi: 10.1038/nprot.2008.211
39. Huang DW, Sherman BT, Lempicki RA. Bioinformatics enrichment tools: paths toward the comprehensive functional analysis of large gene lists. *Nucleic Acids Res.* 2009;37:1–13. doi: 10.1093/nar/gkn923
40. Ashburner M, Ball CA, Blake JA, Botstein D, Butler H, Cherry JM, Davis AP, Dolinski K, Dwight SS, Eppig JT, et al. Gene ontology: tool for the unification of biology. *Nat Genet.* 2000;25:25–29. doi: 10.1038/75556
41. White K, Lu Y, Annis S, Hale AE, Chau BN, Dahlman JE, Hemann C, Opatowsky AR, Vargas SO, Rosas I, et al. Genetic and hypoxic alterations of the microRNA-210-ISCUI/2 axis promote iron-sulfur deficiency and pulmonary hypertension. *EMBO Mol Med.* 2015;7:695–713. doi: 10.15252/emmm.201404511
42. Bertero T, Cottrill KA, Lu Y, Haeger CM, Dieffenbach P, Annis S, Hale A, Bhat B, Kaimal V, Zhang Y-Y, et al. Matrix remodeling promotes pulmonary hypertension through feedback mechanoactivation of the YAP/TAZ-miR-130/301 circuit. *Cell Rep.* 2015;13:1016–1032. doi: 10.1016/j.celrep.2015.09.049
43. Bertero T, Lu Y, Annis S, Hale A, Bhat B, Saggarr R, Saggarr R, Wallace WD, Ross DJ, Vargas SO, et al. Systems-level regulation of microRNA networks by miR-130/301 promotes pulmonary hypertension. *J Clin Invest.* 2014;124:3514–3528. doi: 10.1172/JCI74773
44. Collins T, Korman AJ, Wake CT, Boss JM, Kappes DJ, Fiers W, Ault KA, Gimbrone MA, Strominger JL, Pober JS. Immune interferon activates multiple class II major histocompatibility complex genes and the associated invariant chain gene in human endothelial cells and dermal fibroblasts. *Proc Natl Acad Sci USA.* 1984;81:4917–4921. doi: 10.1073/pnas.81.15.4917
45. Tureson C. Endothelial expression of MHC class II molecules in autoimmune disease. *Curr Pharm Des.* 2004;10:129–143. doi: 10.2174/1381612043453414
46. Karczewski KJ, Francioli LC, Tiao G, Cummings BB, Alföldi J, Wang Q, Collins RL, Laricchia KM, Ganna A, Birnbaum DP, et al. The mutational constraint spectrum quantified from variation in 141,456 humans. *Nature.* 2020;581:434–443. doi: 10.1038/s41586-020-2308-7
47. D'Alonzo GE. Survival in patients with primary pulmonary hypertension. *Ann Intern Med.* 1991;115:343. doi: 10.7326/0003-4819-115-5-343
48. Rubin LJ. Primary pulmonary hypertension. *N Engl J Med.* 1997;336:111–117. doi: 10.1056/NEJM199701093360207
49. Zhao J, Peng W, Ran Y, Ge H, Zhang C, Zou H, Ding Y, Qi H. Dysregulated expression of ACTN4 contributes to endothelial cell injury via the activation of the p38-MAPK/p53 apoptosis pathway in preeclampsia. *J Physiol Biochem.* 2019;75:475–487. doi: 10.1007/s13105-019-00700-9
50. Schaefer A, Te Riet J, Ritz K, Hoogenboezem M, Anthony EC, Mul FPJ, de Vries CJ, Daemen MJ, Figdor CG, van Buul JD, et al. Actin-binding proteins differentially regulate endothelial cell stiffness, ICAM-1 function and neutrophil transmigration. *J Cell Sci.* 2014;127:4470–4482.
51. AksenoVA V, Turoverova L, Khotin M, Magnusson K-E, Tulchinsky E, Melino G, Pinaev GP, Barlev N, Tentler D. Actin-binding protein alpha-actinin 4 (ACTN4) is a transcriptional co-activator of RelA/p65 sub-unit of NF- $\kappa$ B. *Oncotarget.* 2013;4:362–372. doi: 10.18632/oncotarget.901
52. Melton E, Qiu H. Interleukin-1 $\beta$  in multifactorial hypertension: inflammation, vascular smooth muscle cell and extracellular matrix remodeling, and non-coding RNA regulation. *Int J Mol Sci.* 2021;22:8639. doi: 10.3390/ijms22168639
53. Parikh VN, Jin RC, Rabello S, Gulbahce N, White K, Hale A, Cottrill KA, Shaik RS, Waxman AB, Zhang Y-Y, et al. MicroRNA-21 integrates pathogenic signaling to control pulmonary hypertension: results of a network bioinformatics approach. *Circulation.* 2012;125:1520–1532. doi: 10.1161/CIRCULATIONAHA.111.060269
54. Bertero T, Handen AL, Chan SY. Factors associated with heritable pulmonary arterial hypertension exert convergent actions on the miR-130/301-vascular matrix feedback loop. *Int J Mol Sci.* 2018;19:2289. doi: 10.3390/ijms19082289
55. Balda MS, Matter K. Tight junctions at a glance. *J Cell Sci.* 2008;121:3677–3682. doi: 10.1242/jcs.023887
56. Groschwitz KR, Hogan SP. Intestinal barrier function: molecular regulation and disease pathogenesis. *J Allergy Clin Immunol.* 2009;124:3–20; quiz 21. doi: 10.1016/j.jaci.2009.05.038
57. Deng H, Xu Y, Hu X, Zhuang ZW, Chang Y, Wang Y, Ntokou A, Schwartz MA, Su B, Simons M. MEK3-TGF $\beta$  crosstalk regulates inward arterial remodeling. *Proc Natl Acad Sci USA.* 2021;118:e2112625118.
58. Harbaum L, Rhodes CJ, Otero-Núñez P, Wharton J, Wilkins MR. The application of "omics" to pulmonary arterial hypertension. *Br J Pharmacol.* 2021;178:108–120. doi: 10.1111/bph.15056

59. Zhu N, Pauciuolo MW, Welch CL, Lutz KA, Coleman AW, Gonzaga-Jauregui C, Wang J, Grimes JM, Martin LJ, He H, et al. Novel risk genes and mechanisms implicated by exome sequencing of 2572 individuals with pulmonary arterial hypertension. *Genome Med.* 2019;11:69. doi: 10.1186/s13073-019-0685-z
60. Gorlova OY, Xiao X, Tsavachidis S, Amos CI, Gorlov IP. SNP characteristics and validation success in genome wide association studies. *Hum Genet.* 2022; 141:229–238.
61. Wang P, Wang Y, Peng H, Wang J, Zheng Q, Wang P, Wang J, Zhang H, Huang Y, Xiong L, et al. Functional rare variant in a C/EBPbeta binding site in NINJ2 gene increases the risk of coronary artery disease. *Aging (Albany NY).* 2021;13 :25393–25407.
62. Jiang D, Sun W, Wu T, Zou M, Vasamsetti SB, Zhang X, Zhao Y, Tavakoli S, Dutta P, Florentin J, et al. Post-GWAS functional analysis of the CDKN2A/Blocus identifies CUX1 as a regulator of p16INK4a expression and cellular senescence. *Nature Aging.* 2022;2:140–154. doi: 10.1038/s43587-022-00177-0
63. Yang BQ, Assad TR, O'Leary JM, Xu M, Halliday SJ, D'Amico RW, Farber-Eger EH, Wells QS, Hemnes AR, Brittain EL. Racial differences in patients referred for right heart catheterization and risk of pulmonary hypertension. *Pulm Circ.* 2018;8:2045894018764273.
64. Kuebler WM, Nicolls MR, Olschewski A, Abe K, Rabinovitch M, Stewart D, Chan SY, Morrell NW, Archer SL, Spiekerkoetter E. A pro-con debate: current controversies in PAH pathogenesis at the American Thoracic Society international conference in 2017. *Am J Physiol Lung Cell Mol Physiol.* 2018;315:L502–L516. doi: 10.1152/ajplung.00150.2018
65. Pullamsetti SS, Savai R, Seeger W, Goncharova EA. Translational advances in the field of pulmonary hypertension. From cancer biology to new pulmonary arterial hypertension therapeutics. Targeting cell growth and proliferation signaling hubs. *Am J Respir Crit Care Med.* 2017;195:425–437. doi: 10.1164/rccm.201606-1226PP
66. Tentler D, Lomert E, Novitskaya K, Barlev NA. Role of ACTN4 in tumorigenesis, metastasis, and EMT. *Cells.* 2019;8:1427.
67. Peng W, Tong C, Li L, Huang C, Ran Y, Chen X, Bai Y, Liu Y, Zhao J, Tan B, et al. Trophoblastic proliferation and invasion regulated by ACTN4 is impaired in early onset preeclampsia. *FASEB J.* 2019;33:6327–6338. doi: 10.1096/fj.201802058RR
68. Cheng X, Wang Y, Chen H, Xu Y, Xiong W, Wang T. Claudin-1 regulates pulmonary artery smooth muscle cell proliferation through the activation of ERK1/2. *Biomed Pharmacother.* 2017;89:983–990. doi: 10.1016/j.biopha.2017.02.063
69. Bekker V, Chanock SJ, Yeager M, Hutchinson AA, von Hahn T, Chen S, Xiao N, Dotrang M, Brown M, Busch MP, et al. Genetic variation in CLDN1 and susceptibility to hepatitis C virus infection. *J Viral Hepat.* 2010;17:192–200. doi: 10.1111/j.1365-2893.2009.01166.x
70. Battagin AS, Bertuzzo CS, Carvalho PO, Ortega MM, Marson FAL. Single nucleotide variants c.-13G → C (rs17429833) and c.108C → T (rs72466472) in the CLDN1 gene and increased risk for familial colorectal cancer. *Gene.* 2021;768:145304. doi: 10.1016/j.gene.2020.145304
71. Zhang P, Kang B, Xie G, Li S, Gu Y, Shen Y, Zhao X, Ma Y, Li F, Si J, et al. Genomic sequencing and editing revealed the GRM8 signaling pathway as potential therapeutic targets of squamous cell lung cancer. *Cancer Lett.* 2019;442:53–67. doi: 10.1016/j.canlet.2018.10.035
72. Yang D, Jang I, Choi J, Kim M-S, Lee AJ, Kim H, Eom J, Kim D, Jung I, Lee B. 3DIV: a 3D-genome interaction viewer and database. *Nucleic Acids Res.* 2018;46:D52–D57. doi: 10.1093/nar/gkx1017
73. Culley MK, Zhao J, Tai YY, Tang Y, Perk D, Negi V, Yu Q, Woodcock C-SC, Handen A, Speyer G, et al. Frataxin deficiency promotes endothelial senescence in pulmonary hypertension. *J Clin Invest.* 2021;131:131. doi: 10.1172/JCI136459
74. Zehendner CM, Valasarajan C, Werner A, Boeckel J-N, Bischoff FC, John D, Weirick T, Glaser SF, Rossbach O, Jaé N, et al. Long non-coding RNA TYKRIL plays a role in pulmonary hypertension via the p53-mediated regulation of PDGFRβ. *Am J Respir Crit Care Med.* 2020;202:1445–1457. doi: 10.1164/rccm.201910-2041OC
75. Liu G, Betts C, Cunoosamy DM, Åberg PM, Hornberg JJ, Sivars KB, Cohen TS. Use of precision cut lung slices as a translational model for the study of lung biology. *Respir Res.* 2019;20:162. doi: 10.1186/s12931-019-1131-x
76. Opatowsky AR, Hess E, Maron BA, Brittain EL, Barón AE, Maddox TM, Alshawabkeh LI, Wertheim BM, Xu M, Assad TR, et al. Thermodilution vs estimated fick cardiac output measurement in clinical practice: an analysis of mortality from the veterans affairs clinical assessment, reporting, and tracking (VA CART) program and vanderbilt university. *JAMA Cardiol.* 2017;2:1090–1099. doi: 10.1001/jamacardio.2017.2945
77. Yung GL, Fedullo PF, Kinninger K, Johnson W, Channick RN. Comparison of impedance cardiography to direct Fick and thermodilution cardiac output determination in pulmonary arterial hypertension. *Congest Heart Fail.* 2004;10:7–10. doi: 10.1111/j.1527-5299.2004.03406.x
78. Barr PB, Bigdeli TB, Meyers JL. Characterizing and coding psychiatric diagnoses using electronic health record data-reply. *JAMA Psychiatry.* 2022;79:1140. doi: 10.1001/jamapsychiatry.2022.2739
79. Klann JG, Joss MAH, Embree K, Murphy SN. Data model harmonization for the all of us research program: transforming i2b2 data into the OMOP common data model. *PLoS One.* 2019;14:e0212463. doi: 10.1371/journal.pone.0212463



## **SUPPLEMENTAL MATERIAL**

**Table S1. All of Us PAH Database Demographics.** Demographics of 679 PAH patients from All of Us database presented as median [interquartile range] or sample size (%).

***Demographics***

---

Age	67.6 [58.5 – 75.6]
Hospitalizations per year	0.3 [0.0 – 1.4]
Minor allele frequency (A)	0.174
Sex at birth	
Female	351 (64.3%)
Race	
Black or African American	149 (27.3%)
White	367 (67.2%)
Other	30 (5.5%)

---

**Table S2. UPMC Cohort Demographics.** Demographics and other clinical data from 84 PAH patients presented as median [interquartile range] or sample size (%).

***Demographics***

---

Age at catheterization	49.5 [35 – 60]
Sex at birth	
Female	68 (81.0%)
Vasodilator treatment	61 (72.6%)
Mean right atrial pressure (mmHg)	7 [4 – 11]
Mean pulmonary artery pressure (mmHg)	51 [41 – 60]
Pulmonary capillary wedge pressure (mmHg)	10 [7 – 14]
Cardiac output (L/min)	4.39 [3.4 – 5.4]
Cardiac index (L/min/kg/m <sup>2</sup> )	2.3 [1.9 – 2.8]
Pulmonary vascular resistance (Wood units)	9.7 [5.9 – 13.1]

---

**Table S3. Input Sequence for Custom SNP Genotyping.** Custom primers were designed using ThermoFisher custom SNP sequencing tools. Catalog ID: 4332073.

Input	TCAGTTCAAAATATTTTCTAA TTTTCCTTCTGACTCTTTTTAAA TCCAGGTGCTGTTTAGCAGT ATACTTTTTAA TTTCTAGGTA TTTGGGACTTTCAAGGTA TTTTCTGTTA TTGGTTTCTAATTTA ATGCTATTGTGG TCCGAGAA TGTA TTTCTGTA TGA TTTCAATAGAGACA TTTATTTATTTAGACA TTTATTTA TATGTGTTTA TGACCCAGTG TA TAG TCTG TCCTGTGGAA TATTCTTGAGCA TTTGA AAATAATGTGTATTCTGCCACTA TTGGGTGGAATA TTCTACA <b>[G/A]</b> ATCTTGATTAGATCACGT TGGTTCATTGA TAATGTTA TTTAAA TCTA TCA TGT CCTCA TGAAGTTTTTTCCTAAATA TTTTAT TGTTTACTGAGTGCTAGAA TACTAAAATA TAATTGTGAATTTG TCTA TTTTCTGA TTTATTTTTAT CATTTTTGGTA TAATGTGA TTTAAGACATA TTTTCTAAGAACAACACATTTAGGATTGTTATA TGTTGATAATAAAATGATCCTTTTA TCA TTA TGA ACTA TCCTTCTTTCTCCTTGGTAA TATTTCT GAGTCTTATTTTCTGATATTTAA
-------	---

**Table S4. PAH and Control PSMCs Demographics.** Demographics of patients from whom PSMCs were derived. M, male; F, female; IPAH, idiopathic PAH; CTD-PAH, connective tissue disease-associated PAH; FPAH, familial hereditary PAH.

PASMC	Sex	Age (years)	Condition
1	F	33	Non-diseased
2	F	43	Non-diseased
3	F	44	Non-diseased
4	F	50	Non-diseased
5	F	57	Non-diseased
6	F	64	Non-diseased
7	M	25	Non-diseased
8	M	36	Non-diseased
9	M	41	Non-diseased
10	M	53	Non-diseased
11	F	36	IPAH
12	F	40	IPAH
13	F	50	IPAH
14	F	50	CTD-PAH
15	F	53	CTD-PAH
16	F	62	FPAH
17	M	21	IPAH
18	M	31	IPAH
19	M	45	IPAH
20	M	55	IPAH



**Table S5. Ranking of Differential Expressed Genes in PAECs after ACTN4 and HLA-DPA Knockdown.** Transcriptional microarray analysis of RNAs in human PAECs after siRNA mediated ACTN4 and HLA-DPA1 knockdown, sorted by false discovery rate across all conditions. Top 200 genes displayed with their respective average signal and log fold change compared to negative control (siNC).

Gene Symbol	siNC Bi-weight Avg Signal (log2)	siACTN4 Bi-weight Avg Signal (log2)	siHLA-DPA1 Bi-weight Avg Signal (log2)	FDR p-value (All Conditions)	siACTN4 vs siNC (logFC)	siHLA-DPA1 vs siNC (logFC)
KDEL1	13.17	13.8	10.03	0.000001	0.63	-3.14
SEC22B	13.01	11.93	13.55	0.000025	-1.08	0.54
TMEM2	10.47	11.38	9.91	0.000025	0.91	-0.56
LAPTM4A	14.97	14.96	13.31	0.000053	-0.01	-1.66
SERPINB9	13.82	12.39	14.07	0.000056	-1.43	0.25
ERO1A	13.98	15.42	13.53	0.000056	1.44	-0.45
FUT8	11.71	10.79	12.28	0.000056	-0.92	0.57
GLIPR1	15.55	16.71	16.38	0.000061	1.16	0.83
HYOU1	14.46	13.81	11.33	0.000061	-0.65	-3.13
MPZL2	15.13	17.1	16.18	0.000071	1.97	1.05
TMED9	12.05	12.63	11.75	0.000071	0.58	-0.3
FNDC3B	15.78	16.18	14.93	0.000071	0.4	-0.85
RGS5	14.63	11.48	12.61	0.000077	-3.15	-2.02
DUT	11.13	10.77	9.98	0.000077	-0.36	-1.15
MAPK6	11.19	12.72	9.27	0.000077	1.53	-1.92
TPMT	12.48	12.4	10.18	0.000077	-0.08	-2.3
ACTN4	13.91	7.9	14.42	0.000116	-6.01	0.51
CTSL	11.19	13.45	11.74	0.000172	2.26	0.55
EMP3	14.89	15.99	15.96	0.000172	1.1	1.07
UBR4	11.54	14.18	12.68	0.000172	2.64	1.14
BGN	15.9	13.85	14.85	0.000172	-2.05	-1.05
SHTN1	10.14	11.19	9.91	0.000172	1.05	-0.23
ADGRL4	15.19	15.85	14.54	0.000172	0.66	-0.65
HSPA5	15.57	15.96	14.63	0.000172	0.39	-0.94
ITGB5	10.26	10.29	7.47	0.000172	0.03	-2.79
UAP1	12.45	14.57	13.39	0.00019	2.12	0.94
DCBLD2	14.55	15.57	16.76	0.00019	1.02	2.21
AP2M1	13.14	13.51	11.82	0.00019	0.37	-1.32
TMBIM6	16.19	16.91	15.49	0.000193	0.72	-0.7
HYOU1	11.34	11	8.66	0.000193	-0.34	-2.68
CAPNS1	15.25	13.08	15.54	0.0002	-2.17	0.29
ACAA2	10.31	10.62	8.67	0.0002	0.31	-1.64
PGK1	13.04	13.7	13.1	0.000213	0.66	0.06
TOX	10.79	9.44	10.34	0.000213	-1.35	-0.45

NPC1	9.4	11.39	10.63	0.000213	1.99	1.23
RIN2	12.44	10.9	11.43	0.000213	-1.54	-1.01
FAM107A	10.22	8.14	10.59	0.00022	-2.08	0.37
MCFD2	12.76	14.12	13.15	0.00022	1.36	0.39
AP3S1	12.54	10.66	13.26	0.00022	-1.88	0.72
NABP1	10.01	11.48	11.96	0.00022	1.47	1.95
ARCN1	13.67	13.79	12.14	0.00022	0.12	-1.53
CCSER2	13.3	11.7	13.64	0.000221	-1.6	0.34
SELENBP1	5.57	3.92	5.26	0.00023	-1.65	-0.31
GIMAP4	10.46	7.64	9.98	0.00023	-2.82	-0.48
LYPD1	11.28	9.93	8.81	0.00023	-1.35	-2.47
TXNDC9	9.13	10.09	9.67	0.000233	0.96	0.54
MYL9	12.58	13.41	14.43	0.000233	0.83	1.85
TCF4	14.18	13.66	12.56	0.000233	-0.52	-1.62
PRKAA1	13.68	12.46	14.2	0.000237	-1.22	0.52
EBAG9	11.6	9.56	12.08	0.000238	-2.04	0.48
SMURF2	13.53	14.76	13.12	0.000242	1.23	-0.41
OLAH	4.08	7.27	4.34	0.000252	3.19	0.26
GOLPH3L	10.73	9.3	9.43	0.000262	-1.43	-1.3
PSKH1	7.73	5.89	6.86	0.000279	-1.84	-0.87
MTUS1	15.02	12.4	13.44	0.000295	-2.62	-1.58
PLOD2	16.15	17.76	16.64	0.000297	1.61	0.49
CAPZA1	13.69	14.49	12.06	0.000297	0.8	-1.63
WEE1	10.09	11.31	9.26	0.000297	1.22	-0.83
DYNC1H1	12.32	13.14	11.03	0.000297	0.82	-1.29
LDB2	11.11	7.96	8.05	0.000303	-3.15	-3.06
GTF3A	13.24	13.24	10.22	0.000303	0	-3.02
HYOU1	11.61	11.2	8.81	0.000307	-0.41	-2.8
SPOCK1	13.93	11.78	13.12	0.000308	-2.15	-0.81
MAN1A2	11.13	10.36	10	0.000317	-0.77	-1.13
POM121C	11.07	9.56	11.48	0.000317	-1.51	0.41
AES	13.05	13.43	11.81	0.000317	0.38	-1.24
NUCB2	13.75	14.06	12.08	0.000317	0.31	-1.67
SDF4	11.24	11.17	8.38	0.000317	-0.07	-2.86
ANXA1	16.28	17.19	16.69	0.000326	0.91	0.41
HIST1H2AE	11.19	9.44	9.36	0.000326	-1.75	-1.83
HIST1H2AM; HIST1H3J	10.04	8.62	8.31	0.000329	-1.42	-1.73
SEL1L3	13.59	13.93	13.27	0.000329	0.34	-0.32
PPP1R14B	12.64	12.56	11.54	0.000329	-0.08	-1.1
TGFBR2	15.65	13.65	15.58	0.000331	-2	-0.07

RTN4	15.42	16.4	16.33	0.000349	0.98	0.91
PLSCR4	10.9	12.79	11.74	0.000349	1.89	0.84
MAPK3	13.53	12.43	13.82	0.000349	-1.1	0.29
CYB5B	12.63	9.87	12.59	0.000349	-2.76	-0.04
C14orf1	14.05	12.97	14.67	0.000349	-1.08	0.62
MMP2	15.78	14.92	14.47	0.000349	-0.86	-1.31
TMX1	12.59	13.25	12.17	0.000349	0.66	-0.42
ACLY	13.86	14.36	12.5	0.000349	0.5	-1.36
CANX	15.93	15.99	15.23	0.000361	0.06	-0.7
HYOU1	11.72	11.09	8.8	0.000363	-0.63	-2.92
RIT1	10.44	11.98	10.58	0.000371	1.54	0.14
MMRN1	16.63	15.15	16.02	0.000371	-1.48	-0.61
IL6ST	14.29	13.24	10.51	0.000371	-1.05	-3.78
RFTN2	8.27	5.99	6.83	0.000372	-2.28	-1.44
SH3BGRL	11.6	10.64	10.14	0.000372	-0.96	-1.46
STK3	9.35	9.77	8.12	0.000372	0.42	-1.23
HYOU1	10.6	10.14	7.74	0.000372	-0.46	-2.86
PRELID3B; ATP5E	10.27	8.22	10.59	0.000376	-2.05	0.32
PODXL	12.95	14.14	12.36	0.000376	1.19	-0.59
DNASE1L1	11	12.34	10.43	0.000376	1.34	-0.57
HINT1	12.79	12.85	11.8	0.000385	0.06	-0.99
TMEM47	12.46	11.53	12.35	0.000386	-0.93	-0.11
PLAT	10.67	12.57	10.1	0.000386	1.9	-0.57
STEAP1B	11.68	10.15	11.48	0.000386	-1.53	-0.2
SULF1	10.64	7.79	9.41	0.000386	-2.85	-1.23
BAD	8.16	6.3	8.52	0.000386	-1.86	0.36
NQO1	15.33	16.04	15.26	0.000386	0.71	-0.07
SGK1	13.24	14.62	14.77	0.000386	1.38	1.53
TAGLN	10.92	13.09	13.76	0.000386	2.17	2.84
HYOU1	12.32	11.63	9.64	0.000386	-0.69	-2.68
SLC39A6	8.3	10.92	9.36	0.000389	2.62	1.06
CAP1	15.4	16.33	15.99	0.000389	0.93	0.59
CITED2	11.12	10.66	12.29	0.000389	-0.46	1.17
PRNP	12.43	14.82	13.68	0.000403	2.39	1.25
CALCRL	12.82	10.39	11.46	0.000411	-2.43	-1.36
CDCA7L	11.07	9.05	10.15	0.000413	-2.02	-0.92
CEACAM1	7.98	11.53	9.51	0.000413	3.55	1.53
SH3KBP1	10.35	12.66	11.16	0.000413	2.31	0.81
PXK	10.07	7.68	10.34	0.000413	-2.39	0.27
TMEM64	9.69	10.7	8.15	0.000413	1.01	-1.54

PRR11	11.53	8.58	10.77	0.000414	-2.95	-0.76
ARPC4	12.68	11.34	13.11	0.00042	-1.34	0.43
HYOU1	12.37	11.6	9.43	0.00042	-0.77	-2.94
NLGN1	8.17	9.31	7.77	0.000432	1.14	-0.4
GNB4	12.14	13.56	13.17	0.000432	1.42	1.03
HNRNPA1	17.07	16.31	16.49	0.000432	-0.76	-0.58
RAB23	8.52	11.14	10.48	0.000432	2.62	1.96
HYOU1	10.27	9.9	7.51	0.000433	-0.37	-2.76
C12orf57; RNU7-1	10.58	11.15	9.56	0.00044	0.57	-1.02
FAM111A	10.52	9	10.17	0.000449	-1.52	-0.35
SLC25A13	9.68	11.42	10.43	0.000449	1.74	0.75
CREB5	9.24	11.33	9.33	0.000449	2.09	0.09
MAOA	11.11	10.14	8.29	0.000449	-0.97	-2.82
CALD1	13.61	14.7	13.63	0.000449	1.09	0.02
IMPAD1	11.88	12.06	10.1	0.000449	0.18	-1.78
IL1RL1	14.48	16.25	15.37	0.00045	1.77	0.89
SNAI1	8.17	10.56	8.06	0.00045	2.39	-0.11
ARHGAP18	11.69	10.44	9.47	0.00045	-1.25	-2.22
SNX3	11.76	12.27	9.89	0.00045	0.51	-1.87
DNAJB4	14.74	13.55	15.06	0.000452	-1.19	0.32
CCNYL1; MIR4775	11.31	9.45	11.48	0.000454	-1.86	0.17
CD69	4.89	9.78	6.24	0.00046	4.89	1.35
TLL5	11.66	10.74	12.26	0.000469	-0.92	0.6
NETO2	10.4	11.88	8.95	0.000469	1.48	-1.45
SORBS2	11.79	9.92	12.22	0.000475	-1.87	0.43
OSTM1	10.16	11.48	9.28	0.000487	1.32	-0.88
IPO5	10.97	8.83	10.71	0.000487	-2.14	-0.26
WDR1	14.86	15.89	15.76	0.000488	1.03	0.9
BMP6	14.15	13.37	13.88	0.000498	-0.78	-0.27
PSMC2	14.08	14.78	14.63	0.000506	0.7	0.55
DUSP1	9.51	11.8	11.91	0.000506	2.29	2.4
PEX11B	10.64	9.62	11.53	0.000506	-1.02	0.89
HYOU1	12.8	12.19	9.63	0.000506	-0.61	-3.17
CDIPT	11.13	9.67	11.32	0.000509	-1.46	0.19
CLDN1	5.31	12.19	7.93	0.000509	6.88	2.62
HIST1H2AJ	15.35	13.85	13.67	0.000509	-1.5	-1.68
EIF3J	12.08	12.88	11.52	0.000509	0.8	-0.56
MTAP	8.05	8.94	7.19	0.000509	0.89	-0.86
HIST1H4H	8.91	8.23	7.45	0.000509	-0.68	-1.46

HIST1H1E	13.49	11.74	11.84	0.00052	-1.75	-1.65
GRPEL2	11.62	13.63	11.82	0.000521	2.01	0.2
RNF38	11.6	9.5	11.78	0.000521	-2.1	0.18
TMED7- TICAM2; TICAM2; TMED7	13.68	14.25	12.79	0.000539	0.57	-0.89
ABCA8	10.08	8.04	8.96	0.00055	-2.04	-1.12
GOLIM4	11.61	11.42	10.3	0.00055	-0.19	-1.31
COPS8	13.35	12.64	14.39	0.000558	-0.71	1.04
TM6SF1	10.63	12.23	11.17	0.000564	1.6	0.54
TMEM123	15.94	14.2	16.29	0.000564	-1.74	0.35
ATP6V1B2	11.61	13.02	12.87	0.000564	1.41	1.26
MT1E	16.55	17.32	17.59	0.000564	0.77	1.04
ASNS	7.39	8.99	7.26	0.000576	1.6	-0.13
CCL2	14.87	12.94	13.84	0.000576	-1.93	-1.03
DUSP3	10.91	12.76	11.74	0.000576	1.85	0.83
PDE7B	9.69	6.44	9.05	0.000576	-3.25	-0.64
HIST1H2BM	14.23	12.22	11.96	0.000576	-2.01	-2.27
HYOU1	10.32	9.85	7.47	0.000576	-0.47	-2.85
DUSP16	6.83	8.45	7.32	0.000593	1.62	0.49
CLTB	11.68	13	11.95	0.000593	1.32	0.27
EIF4EBP2	12.9	10.67	12.81	0.000605	-2.23	-0.09
MGP	13.08	10.46	12.11	0.000605	-2.62	-0.97
ZNF148	10.44	9.33	10.49	0.000605	-1.11	0.05
NRP1	14.07	13.4	13.3	0.000605	-0.67	-0.77
TNFSF10	11.65	9.34	10.52	0.00063	-2.31	-1.13
VAT1	13.9	15.14	14.29	0.00063	1.24	0.39
TMEM154	9.48	12.17	9.98	0.00063	2.69	0.5
CSGALNACT2	8.28	9.63	8.8	0.00064	1.35	0.52
EFHD2	10.31	11.75	11.55	0.00064	1.44	1.24
OTUD5	9.63	9.75	8	0.00064	0.12	-1.63
DCTN6	10.79	11.29	9.05	0.000655	0.5	-1.74
EZR	14.21	13.43	14.62	0.000659	-0.78	0.41
MSN	15.95	16.45	16.88	0.000663	0.5	0.93
RNF149	9.69	11.28	10.52	0.000667	1.59	0.83
XPR1	11.28	10.26	11.33	0.000667	-1.02	0.05
EFNB2	9.2	8.12	7.39	0.000667	-1.08	-1.81
CCND1	13.48	12.7	14.74	0.000667	-0.78	1.26
SYPL1	10.18	10.77	8.83	0.000667	0.59	-1.35
RAP2C	9.58	10.09	7.07	0.000667	0.51	-2.51



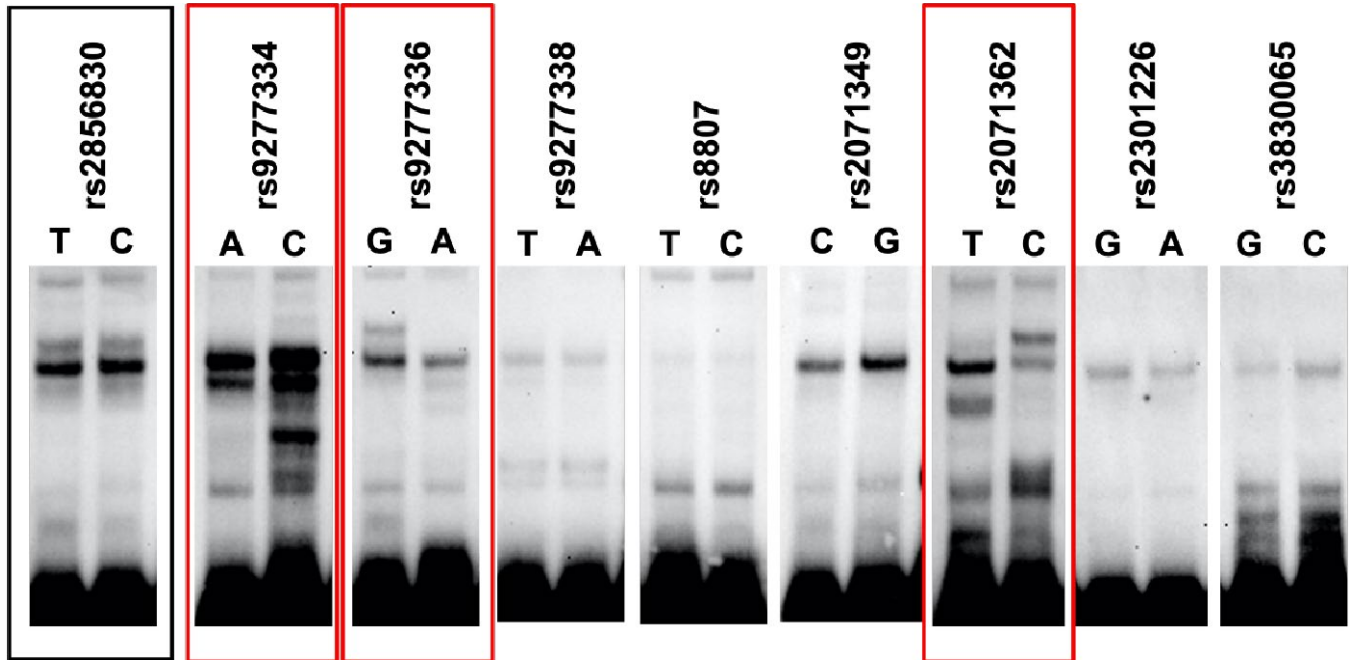
DNAJC3	11.33	11.76	10.4	0.000669	0.43	-0.93
FAF2	12.32	13.06	12.71	0.000672	0.74	0.39
PLP2	16	15.14	16.22	0.000672	-0.86	0.22
BPNT1	9.32	7.47	9.36	0.000672	-1.85	0.04
BTBD7	9.66	8.36	10.2	0.000672	-1.3	0.54
CALR	17.45	17.63	16.77	0.000672	0.18	-0.68
SMARCC2	13.9	12.66	13.38	0.000688	-1.24	-0.52
KDM3B	8.91	7.53	8.93	0.000688	-1.38	0.02
TBC1D2	6.2	9.26	8.01	0.000691	3.06	1.81

**Table S6. Pulmonary Hypertension Network Genes.** List of 756 genes defined and previously validated<sup>40</sup> as a network of downstream PH related effectors derived from literature search and molecular interaction database mining. This list was used to create **Figure S4A-B**.

A2M	BMP7	CSPG4	FBXO6	HSPE1	MIR145	PDGFRA	RTN4	TEK
AAMP	BMPR1A	CST4	FBXW11	HTR1A	MIR17	PDGFRB	RYK	TERT
AARSD1	BMPR1B	CTBP1	FDPS	HTR1B	MIR21	PDGFRL	RYR2	TFIP11
ABAT	BMPR2	CTGF	FGL1	HTR1D	MIR27A	PDHA1	S100A4	TGFB1
ABCC4	BRD4	CTH	FHL1	HTR2B	MIR328	PDK1	S100A7	TGFBI
ABHD5	C3	CTNNB1	FLNA	ICAM1	MIR424	PDK2	S1PR1	TGFBR1
ACE	CA8	CTSD	FLOT1	ID1	MIR503	PDK3	SAE1	TGFBR2
ACE2	CACNA1C	CX3CL1	FN1	ID2	MIRLET7A 1	PDK4	SARAF	TGFBR3
ACLY	CALCOCO 2	CX3CR1	FOS	IDO1	MIRLET7B	PDZK1	SCN5A	TH
ACO1	CALM1	CXCL10	FOSL2	IGF1R	MIRLET7C	PEBP1	SEC31A	THBS1
ACP5	CALM2	CXCL12	FOXF1	IKZF1	MIRLET7D	PEX19	SELP	TIMM21
ACPP	CALM3	CXCR6	FOXI2	IL13	MIRLET7E	PEX5	SEMA3F	TIMP1
ACTA2	CALML5	CYBA	FOXO1	IL13RA2	MKL1	PFKM	SENP1	TINAGL1
ACTB	CALR	CYP19A 1	FOXO3	IL1A	MLYCD	PHF1	SERPINA 1	TLR4
ACTG2	CAMK2D	CYP1B1	FSD1	IL1B	MME	PIM1	SERPINB 8	TMEM17
ACTN1	CAMKK1	CYTH2	FYCO1	IL1R1	MMP1	PKM	SERPINE 1	TMEM216
ACTN2	CAND1	DAG1	FYN	IL6	MMP2	PLA2G4A	SFN	TMEM30 A
ACTN3	CAPN1	DDIT3	FYTDD1	ILVBL	MMP3	PLA2G4B	SGTA	TNC
ACTN4	CAPN2	DDX24	GAN	INS	MMP9	PLIN1	SH3BP4	TNF
ACVRL1	CAPN6	DDX3Y	GATA2	IRF4	MPG	PLP2	SH3GL2	TNFRSF2 5
ADA	CAPNS1	DES	GATA3	ISCU	MRPL50	PMEPA1	SHBG	TNFSF10
ADORA2A	CASP8	DFFA	GCH1	ISYNA1	MST1	PNPLA2	SHROOM 1	TNFSF11
AGER	CASP9	DHDDS	GDF15	ITGAV	MT1G	POLB	SH2B2	TNFSF12
AGT	CASR	DLD	GDF2	JAK1	MT2A	POLR2F	SIN3B	TNFSF13 B
AGTR1	CAT	DLG1	GDF5	JMJD7- PLA2G4B	MTOR	POU5F1	SIRT3	TNFSF4
AGTRAP	CAV1	DLG2	GHRL	JUN	MYC	PPARG	SIRT4	TOPBP1
AHSA1	CAV3	DLG3	GIT2	KBTBD7	NAF1	PPARGC1 A	SKAP2	TP53
AK2	CBL	DLG4	GLI1	KCNA5	NAMPT	PPID	SLAMF1	TP53RK
AKR1B1	CBS	DNAJB1	GLI3	KCND2	NCKIPSD	PPM1B	SLC25A3 2	TPD52L2
AKT1	CBX4	DNM1L	GLO1	KCND3	NCOA2	PRDM14	SLC25A4 1	TPH1
ALB	CCDC8	DPF2	GLS	KCNE4	NCOA3	PREP	SLC37A1	TRAF2
ALOX5	CCL19	DSTN	GNAT1	KCNIP1	NCOR1	PRF1	SLC6A4	TRIM23
AMIGO2	CCL2	DTYMK	GOLGA2	KCNIP2	NDRG1	PRG2	SLC9A1	TRIM59
AMIGO3	CCL3	DUSP1	GORAB	KCNK3	NEDD4	PRKAA2	SLC9A3R 1	TRPC1
ANGPT1	CCL5	DUSP7	GP1BA	KDM4A	NEDD4L	PRKACA	SLC9A3R 2	TRPC3
ANGPT2	CCND1	DUT	GPBR1	KDR	NEFH	PRKAR2A	SMAD1	TRPC4
ANGPT4	CCND3	DVL1	GRB2	KEL	NEK6	PRKAR2B	SMAD2	TRPC6
ANGPTL1	CCNE1	DVL2	GREM1	KLF4	NFATC2	PRKCA	SMAD3	TRPV4
ANK3	CCR1	DVL3	GSTK1	KLF5	NFATC3	PRKD2	SMAD4	TSC1
ANKRD13 A	CCR7	DYNLT1	GUCY1A2	KLHL1	NFKB1	PRKG1	SMAD5	TSHZ1
ANO1	CCRL2	DYSF	GUCY1A3	KRT31	NFKB2	PRKG2	SMAD6	TSPAN10
AP1B1	CD209	E2F4	GUCY1B3	KRT40	NFS1	PRL	SMAD7	UBA7

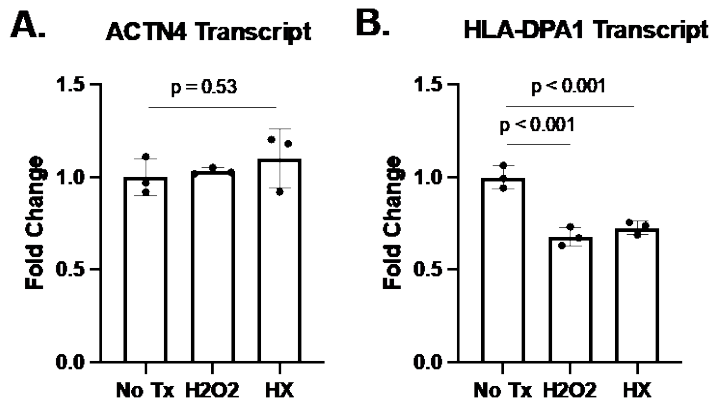
AP1M1	CD226	EBAG9	GZMB	LAMB2	NFU1	PRMT1	SMAD9	UBC
AP2A1	CD4	ECE1	HAS2	LEP	NME1-NME2	PRMT3	SMURF1	UBD
APBB1	CD40LG	ECH1	HAX1	LEPR	NME2	PRMT5	SMYD3	UBE2O
APEH	CD44	EDN1	HDAC1	LGALS1	NME6	PSMA1	SNAPIN	UBE3A
APLN	CD47	EDN2	HDAC11	LGALS3	NOG	PSMA3	SNRNP70	UBQLN4
APLNR	CD74	EDN3	HDAC4	LGALS8	NOL3	PSTPIP1	SNTA1	UNC119
APOA1	CD82	EDNRA	HDAC5	LGALS9C	NOMO1	PTBP1	SNTB1	USP4
APOBEC3C	CDC25A	EDNRB	HES5	LIMK1	NOS1	PTEN	SNTB2	UTS2
APOD	CDC37	EEF1A1	HEXIM1	LLGL2	NOS2	PTGDS	SNX11	UTS2R
APOE	CDK2	EFNA1	HGF	LNX1	NOS3	PTGIR	SNX17	VANGL1
APP	CDK6	EGF	HIF1A	LOX	NOTCH1	PTGIS	SNX3	VCAM1
AR	CDKN1B	EGFR	HIRA	LOXL1	NOTCH3	PTGS2	SOCS7	VCAN
ARG1	CDKN2A	EGR1	HK2	LOXL2	NOX4	PTMA	SOD2	VEGFA
ARG2	CDKN2D	EIF2AK4	HLA-B	LOXL3	NPHP1	PTP4A3	SP1	VHL
ARHGEF12	CEBPB	EIF3E	HLA-DPA1	LOXL4	NPHP3	PTPN3	SP3	VIP
ARIH2	CEP164	EIF3F	HLA-DPB1	LPAR1	NPPB	PTPRK	SPHK1	VIPR1
ATF2	CFL1	ELAVL1	HLA-DQB1	LRP1	NRAS	PTX3	SPINT2	VIPR2
ATF4	CFL2	ELN	HLA-DRB1	LRP2	NRIP1	QKI	SPP1	VKORC1
ATF6	CFTR	ENG	HLA-DRB5	LRP8	NT5C3A	RACK1	SPRY2	VWF
ATIC	CLDN4	ENO2	HMGCR	LYN	NTRK1	RAE1	SRC	WBP1
ATP12A	CLEC4G	ENTPD1	HMOX1	LYST	NUP62	RAF1	SRD5A1	WDR1
ATP1B1	CLIC4	EPAS1	HMOX2	MAOA	NUS1	RAN	SRF	WDYHV1
ATP2A2	CLK1	EPB41L3	HNF4A	MAP2K1	NUTF2	RBL2	SRGN	WNT1
ATP2B1	CMA1	EPM2A	HPRT1	MAP2K4	NYX	RBPJ	SRI	WNT5A
ATP2B2	CNDP1	ERAL1	HSD17B1	MAP2K5	OS9	RBPMS	SRPK1	WWP2
ATP2B3	CNDP2	ERBIN	HSD17B10	MAP3K2	OTUB1	RECK	SS18L2	XBP1
ATP2B4	CNR1	ERG	HSD17B11	MAP4	PACSIN2	RELA	SSSCA1	XDH
ATP5A1	COL1A1	ESR1	HSD17B12	MAPK1	PACSIN3	RFX1	STAT1	XIAP
ATP6V1B2	COL1A2	ESR2	HSD17B13	MAPK10	PAPSS2	RFXAP	STAT3	XPO1
ATP8B4	COL3A1	ESRRA	HSD17B14	MAPK12	PARK2	RGS16	STAT4	XPO5
ATXN1	COL4A1	ESRRB	HSD17B2	MAPK14	PATJ	RGS19	STAT5A	YAP1
AZGP1	COL4A2	ESRRG	HSD17B3	MAPK8	PBRM1	RGS2	STK17B	YWHAB
B2M	CPB2	EVC2	HSD17B4	MAPK9	PCBP1	RGS3	SUMO2	YWHAZ
BANP	CPS1	EWSR1	HSD17B6	MAX	PCBP4	RHOA	TAC1	ZADH2
BCAR3	CREB3	EZR	HSD17B7	MDF1	PCDH20	RHOB	TAGLN	ZC3H12A
BCL2	CRHR1	F11R	HSD17B8	MDM2	PDE10A	RMND5B	TAZ	ZNF197
BIRC2	CRMP1	F2R	HSP90AA1	MEF2A	PDE1A	ROCK1	TBX21	ZNF589
BMP10	CRP	F2RL1	HSP90AB1	MEOX2	PDE3A	ROCK2	TBXA2R	ZNFX1
BMP2	CSNK1G1	FAM9B	HSPA5	MFN2	PDE5A	RPE	TCTA	ZPR1
BMP4	CSNK2A1	FBXO15	HSPA8	MID2	PDGFA	RPL29	TCTN2	ZRANB2
BMP6	CSNK2B	FBXO32	HSPB1	MIR130A	PDGFB	RTEL1	TCTN3	ZSCAN32

**Figure S1. Differential nuclear protein binding to major and minor alleles to some of the 8 SNPs in linkage disequilibrium with SNP rs2856830.**



Electrophoretic mobility shift assays of human PAEC nuclear protein extract binding to oligonucleotides corresponding with the major and minor alleles of all 8 SNPs in linkage disequilibrium ( $r^2 > 0.80$ ) with the original tag SNP rs2856830 in black box and SNPs with differential binding of proteins in red boxes.

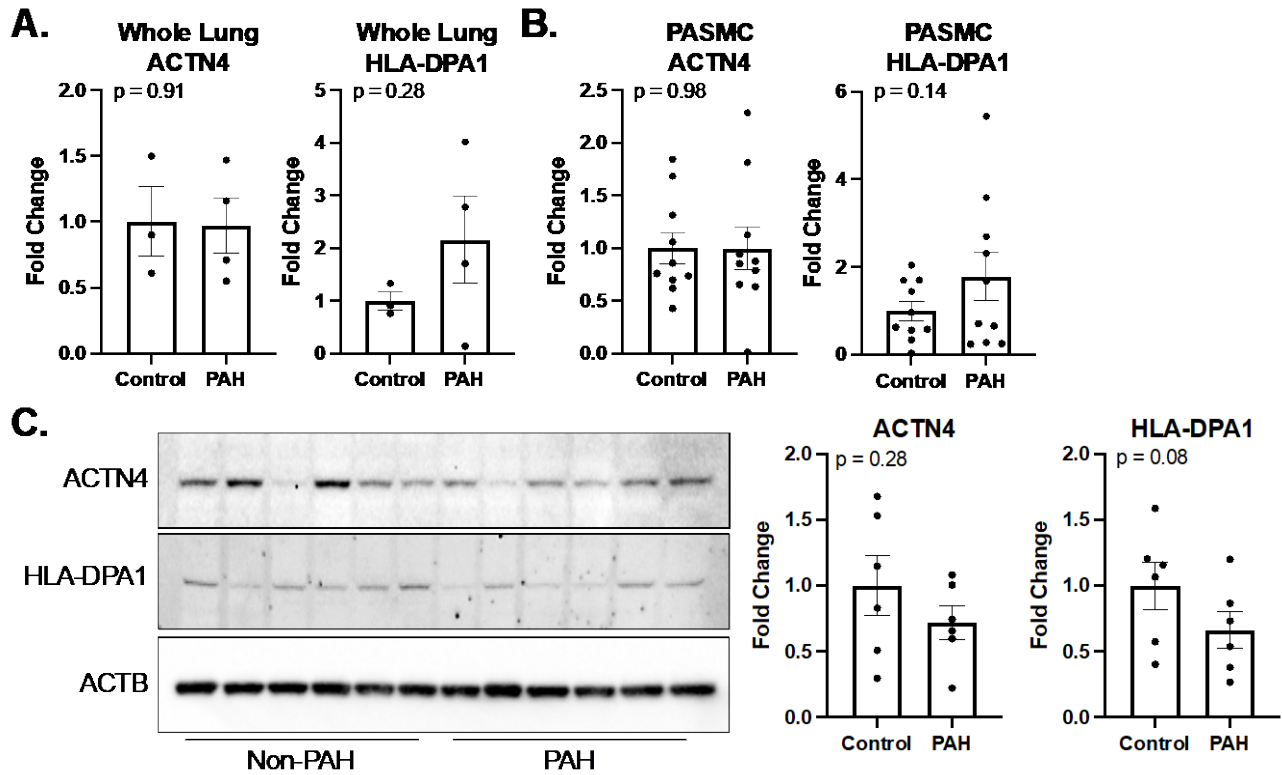
**Figure S2. Hydrogen peroxide and hypoxia variably affects HLA-DPA1 transcript expression, but not ACTN4 in human PAECs.**



**A-B.** ACTN4 and HLA-DPA1 transcript expression under no treatment (NT), 50  $\mu$ M hydrogen peroxide ( $H_2O_2$ ) and 48-hours of hypoxia (HX) exposure as assessed by RT-qPCR. Data are represented as mean  $\pm$  SEM. Significance determined by permuted ANOVA. n=3.

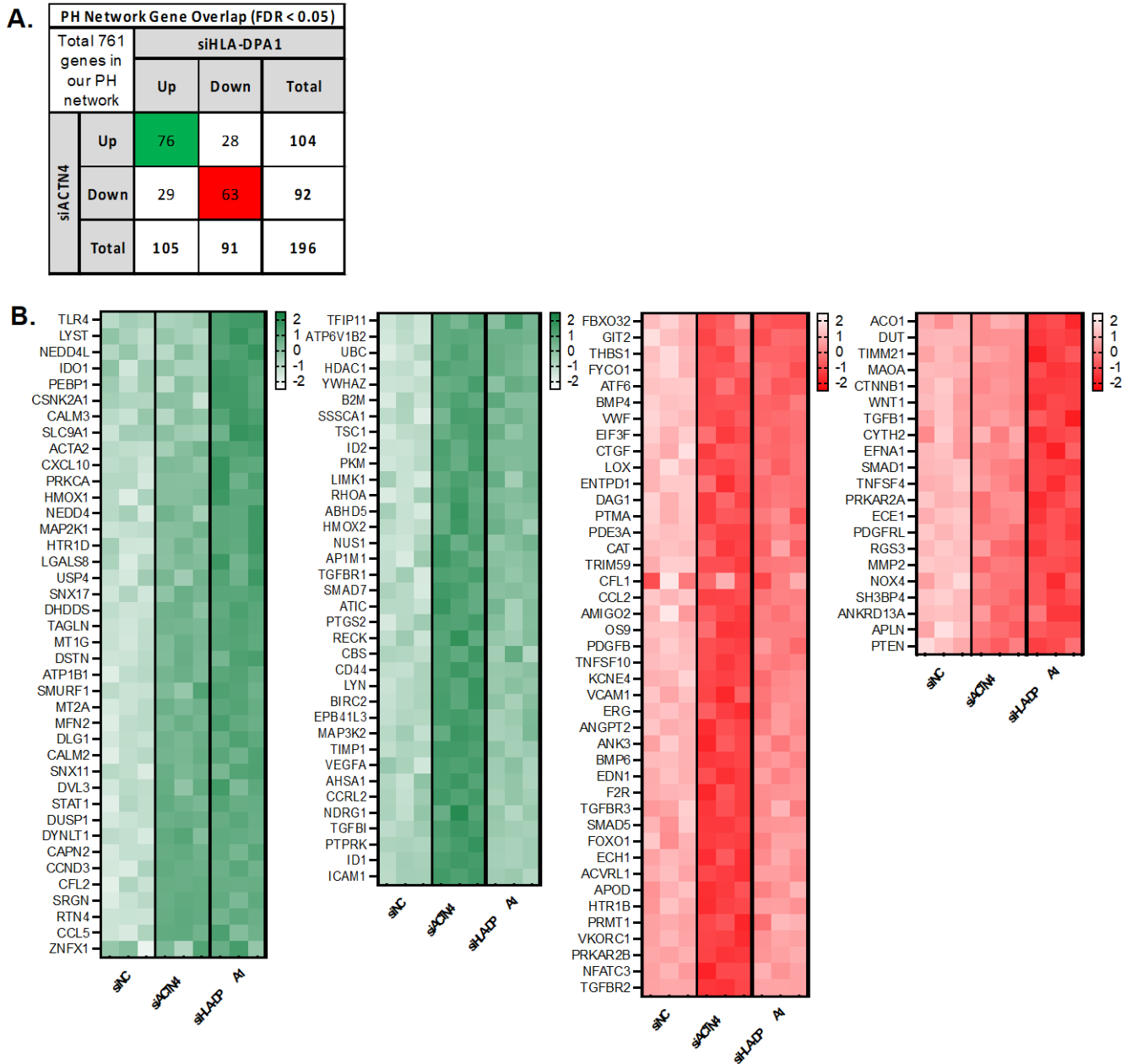


**Figure S3. No difference in ACTN4 and HLA-DPA1 expression in whole lung homogenates and PASMCs derived from PH patients.**



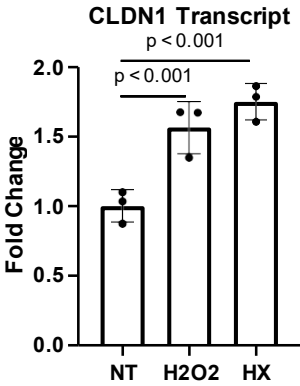
**A-B.** ACTN4 and HLA-DPA1 expression in whole lung homogenates and pulmonary arterial smooth muscle cells (PASMCs) of non-PAH control and PAH patients as assessed by RT-qPCR. **C.** ACTN4 and HLA-DPA1 expression in PASMCs isolated from non-PAH control and PAH patients as assessed by immunoblotting. Beta-actin (ACTB) loading control. Representative data are represented as mean  $\pm$  SEM. Significance determined by permuted t-test.

**Figure S4. Microarray of ACTN4 and HLA-DPA1 knockdown revealed altered gene expression within the known PAH gene network.**



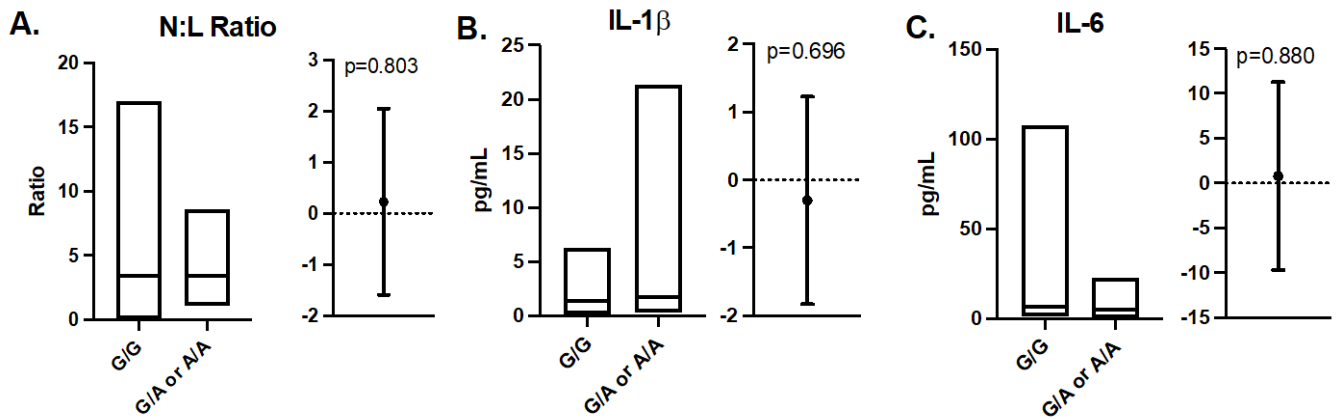
**A.** Summary table of number of genes with significant alterations based on microarray of ACTN4/HLA-DPA1 knockdown conditions in human PAECs and with overlap with a known PAH gene network<sup>40</sup>. **B.** Heat map depicting genes within known PAH network with significant unidirectional expression shifts between microarray of ACTN4 and HLA-DPA1 knockdown conditions in human PAECs. n=3.

**Figure S5. Hydrogen peroxide and hypoxia increases CLDN1 transcript expression in human PAECs.**



CLDN1 transcript expression under no treatment (NT), 50 μM hydrogen peroxide (H<sub>2</sub>O<sub>2</sub>) and 48-hours of hypoxia (HX) exposure as assessed by RT-qPCR. Data are represented as mean ± SEM. Significance determined by permuted ANOVA. n=3.

**Figure S6. SNP rs9277336 genotype effect on inflammatory markers among UPMC PH cohort.**



**A.** Left panel shows median (IQR) of neutrophil to lymphocyte (N:L) ratio in collected CBC blood draw at time of diagnosis pulled from patient medical records; right panel shows 95% confidence interval of parameter adjusted for age, sex, and vasodilator treatment. **B-C.** Left panels show median (IQR) of interleukin-1 $\beta$  (IL-1 $\beta$ ) and interleukin-6 (IL6) plasma quantification by ELISA; right panel shows 95% confidence interval of parameter adjusted for age, sex, and vasodilator treatment. Significance determined by a robust sandwich variance estimator.